NASA TECHNICAL MEMORANDUM

NASA TM X-2078

NASA TM X-2078

NEUTRON KINETICS OF A FAST, HOT, CRITICAL ASSEMBLY IN THE STARTUP MODE

by George F. Niederauer

Lewis Research Center

Cleveland, Ohio 44135

NATIONAL AERONAUTICS AND SPACE ADMINISTRATION • WASHINGTON, D. C. • SEPTEMBER 1970

1. Report No. NASA TM X-2078	2. Government Accession No.	3. Recipient's Catalog No.
4. Title and Subtitle NEUTRON KINETICS OF A FAST, HOT, CRITICAL ASSEMBLY IN THE STARTUP MODE		5. Report Date September 1970 6. Performing Organization Code
7. Author(s) George F. Niederauer		8. Performing Organization Report No. E-5289
9. Performing Organization Name and Address Lewis Research Center National Aeronautics and Space Administration Cleveland, Ohio 44135		10. Work Unit No. 120-27 11. Contract or Grant No. 13. Type of Report and Period Covered Technical Memorandum
12. Sponsoring Agency Name and Address National Aeronautics and Space Administration Washington, D.C. 20546		14. Sponsoring Agency Code

15. Supplementary Notes

16. Abstract

A reactor for auxiliary power in space has been designed using $U^{235}N$ fuel in a tantalum structure with Li^{7} coolant. The kinetics of a hot ($\geq$460 K; 828° R) critical assembly of the same design with and without coolant has been parametrically studied in the startup mode to determine safe operating ranges of ramp reactivity inputs. The main parameters considered were wide ranges in the magnitudes of the Doppler and thermal expansion reactivity coefficients and several kinds of expansion effects.

17. Key Words (Suggested by Author(s))	18. Distribution Statement
Liquid-metal reactor; Fast reactor; Reactor safety; Reactor physics; Kinetics; Reactivity effects; Dynamics; Reactor analysis; Accident analysis; and Transient response	Unclassified - unlimited

19. Security Classif. (of this report)	20. Security Classif. (of this page)	21. No. of Pages	22. Price*
Unclassified	Unclassified	44	$3.00

*For sale by the Clearinghouse for Federal Scientific and Technical Information
Springfield, Virginia 22151

CONTENTS

	Page
SUMMARY	1
INTRODUCTION	1
THE HOT CRITICAL ASSEMBLY	2
Description	2
Time Constants	7
Reactivity Coefficients	8
KINETICS WITH COOLANT	10
Model	10
Equations	12
Results	14
Steady-state	14
Kinetics of reference model	16
Variations on the reference model	22
KINETICS WITHOUT COOLANT	29
Model	29
Equations	30
Results	32
Steady-State	32
Transients	34
CONCLUSIONS	38
APPENDIXES:	
A - SYMBOLS	39
B - DOPPLER COEFFICIENTS	40
REFERENCES	42

NEUTRON KINETICS OF A FAST, HOT, CRITICAL ASSEMBLY IN THE STARTUP MODE

by George F. Niederauer

Lewis Research Center

SUMMARY

The kinetics of a hot (≥460 K; 828° R), critical assembly (HCA) of uranium-235 nitride ($U^{235}N$) fuel in a tantalum structure with lithium-7 (Li^7) coolant has been studied in the startup mode to determine safe operating ranges of reactivity input. A realistic and yet conservative set of reactivity input limits that will prevent possible fuel melting are shown in the following table:

HCA system	Ramp reactivity input limits	
	Maximum level, $	Rate, ¢/sec
With coolant	3.1 .98	<9 >9
Without coolant	0.97	All

The critical ramp rate (9 ¢/sec) and the maximum safe reactivity insertion at rates above the critical rate are not affected by wide variations in the reactivity coefficients. The maximum reactivity input level for rates less than 9 cents per second (¢/sec) may be substantially increased when more information on the Doppler effect and on axial bulging of the fuel assemblies is found.

INTRODUCTION

Reactors developed for space auxiliary power applications need a higher temperature

operating capability than do present reactors. One way of achieving higher temperatures is to use the refractory metal tantalum to contain the nuclear fuel and to support the core. Using fully enriched uranium-235 nitride (UN) fuel and a lithium-7 (Li^7) coolant results in a fast-spectrum reactor which has a short mean neutron lifetime (about 50 nsec).

Little is known about the operating limits of such a system. It is the purpose of this report to determine some preliminary limits of reactivity insertion. The information necessary for refined calculations will come from experiments. In a hot critical assembly (as differentiated from one run at room temperature) experiments would be conducted at temperatures above the Li^7 melting point (460 K; 828° R). A hot critical assembly (HCA) would provide an experimental determination of thermal expansion effects, Doppler broadening, and perhaps fuel-element bowing. However, it is important to determine first the safety of an HCA.

In this regard preliminary reactor kinetic studies have been carried out using a modified version of the AIROS reactor dynamics code (ref. 1). The studies have been de signed to map the kinetic characteristics of an HCA and to determine safe operating limits of reactivity input. The main concern has been on the maximum rate and level of reactivity input for an HCA in a startup situation. This condition was chosen because it. was presumed to have the greatest potential for being the least safe operating mode.

The reference startup case for these studies is an HCA with an initial temperature everywhere of 461 K (830° R) (to maintain the coolant in the liquid state), with zero initial reactivity (reactor just critical), and with low neutron and precursor populations (1 neutron per cubic centimeter (n/cm^3), equivalent to 20 W of thermal power).

To allow for variances in the thermal expansion coefficients and for a wide range in the value of Doppler coefficients, these effects have been studied parametrically. Control operation is approximated by ramp inputs of reactivity, and a wide range of operations have been investigated to determine the safe operating limits of these controls.

The next section describes the HCA and some of its characteristics that are important to safety studies. This will be followed by a discussion of the investigation, which is divided into two almost independent parts: kinetics with coolant and kinetics without coolant.

HOT CRITICAL ASSEMBLY

Description

Two assemblies are described here, one with an external sliding reflector control and the other with an internal fuel-reflector drum control. The sliding reflector control was carried throughout the kinetics study of the HCA with coolant. For the second study,

kinetics without coolant, the model of the whole reactor was changed to the drum control design. Since the reactor core is treated by point reactor kinetics and since heat transport out of the core is slow compared with temperature transients in the core for large, fast reactivity inputs, thermal effects outside the core are insignificant to the outcome of these studies.

A cross section of the reflector-controlled reactor is shown in figure 1 and of the

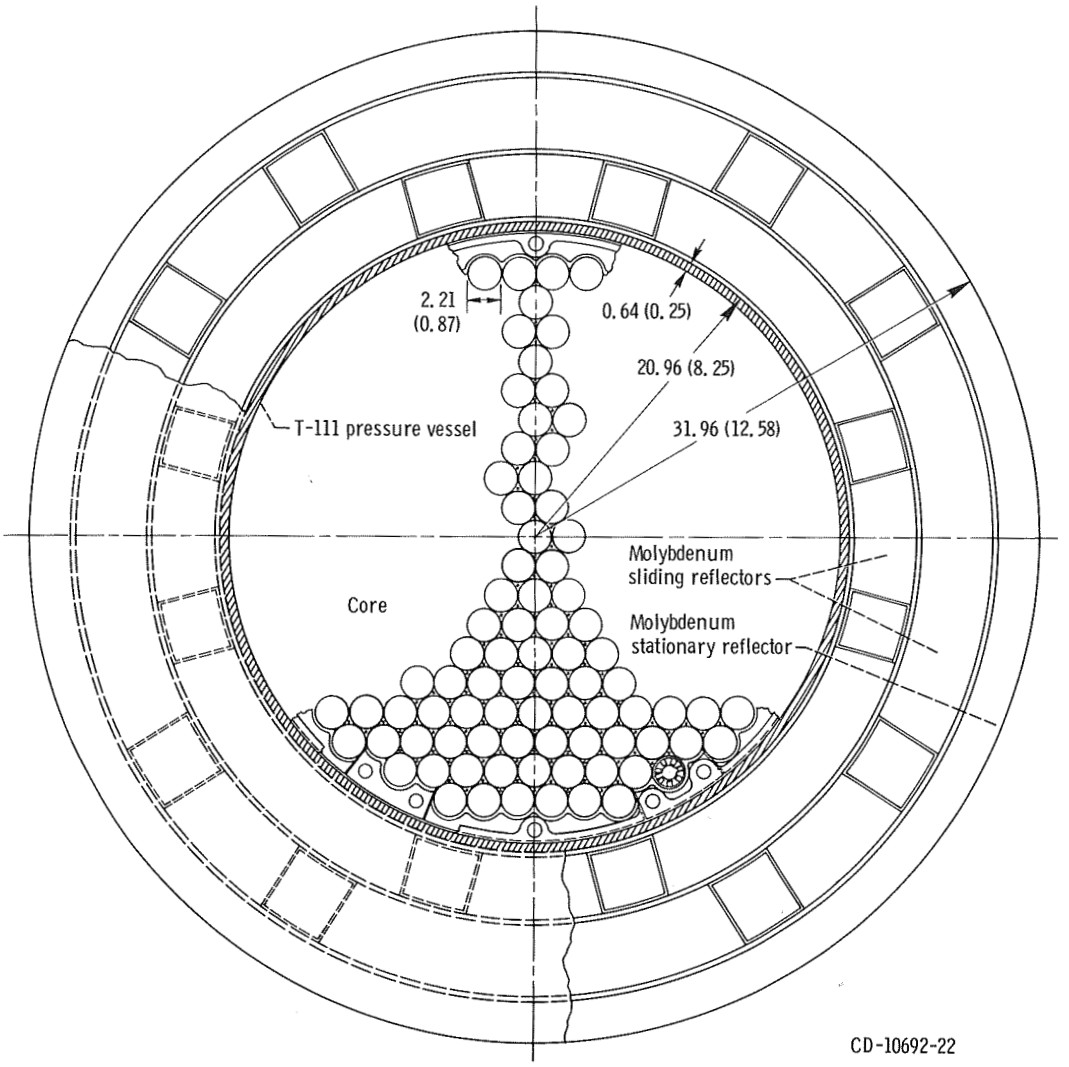

Figure 1. - Sliding reflector-controlled reactor cross-section. (All dimensions are in centimeters (in.).)

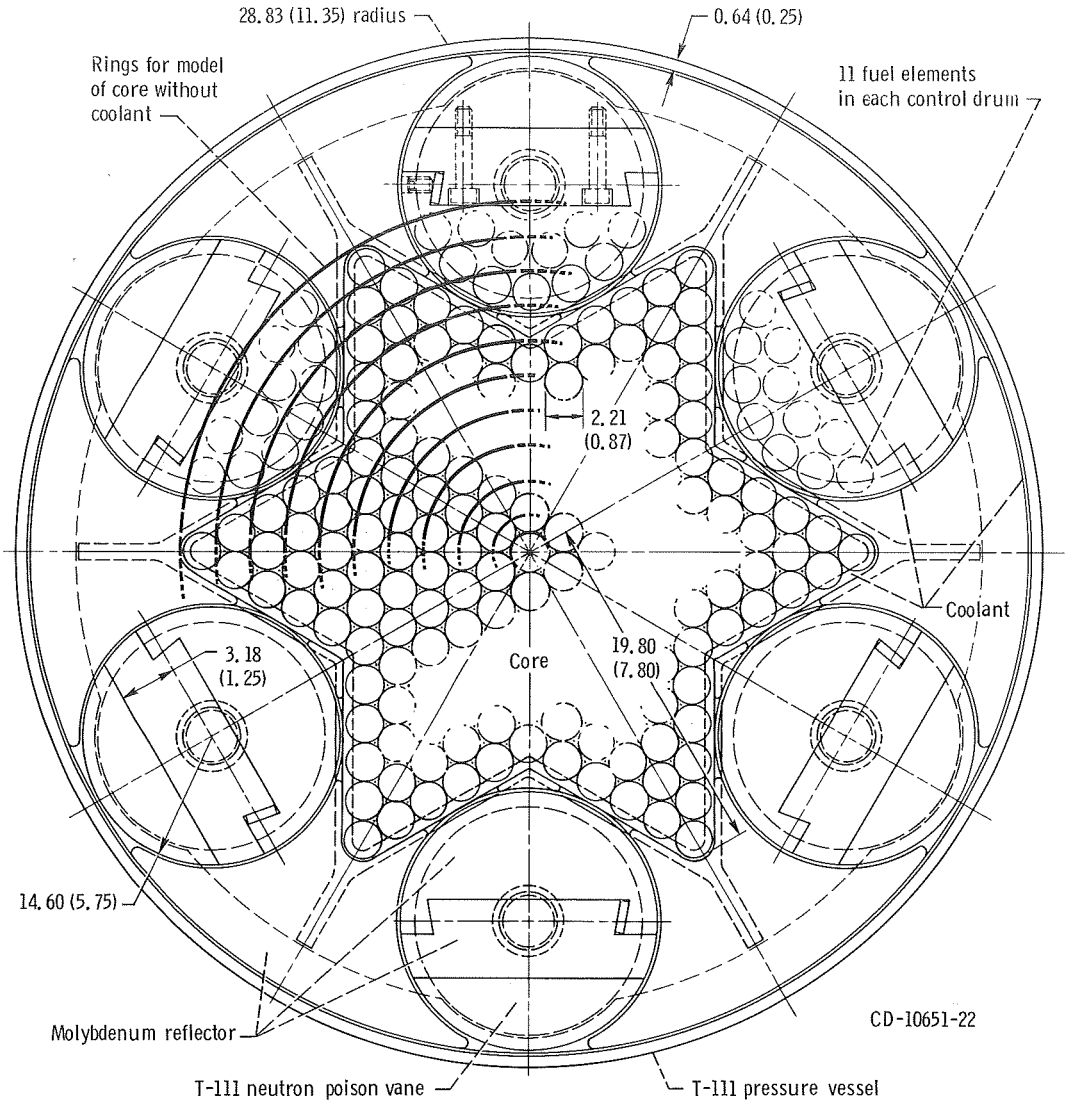

(a) Radial cross section.

Figure 2. - Drum-controlled reactor. (All dimensions are in centimeters (in.).)

drum-controlled reactor in figure 2. A side view of the drum-controlled reactor is shown in figure 2(b). Both core models have identical cellular structure; one cell is shown in figure 3. The core is fueled with hollow cylinders of fully enriched $U^{235}N$, which are surrounded by T-111 (89.2 wt. % Ta - 8.5 wt. % W - 2.3 wt. % Hf) lined on the inside with tungsten. The fuel elements are alined in the T-111 honeycomb supporting structure by dimples on the T-111 tubes. The HCA reactor vessel is not connected to any external coolant loops. Therefore, the coolant remains stagnant in the vessel. The Li^7 coolant, when present in the HCA, lies primarily in the annular coolant channels but

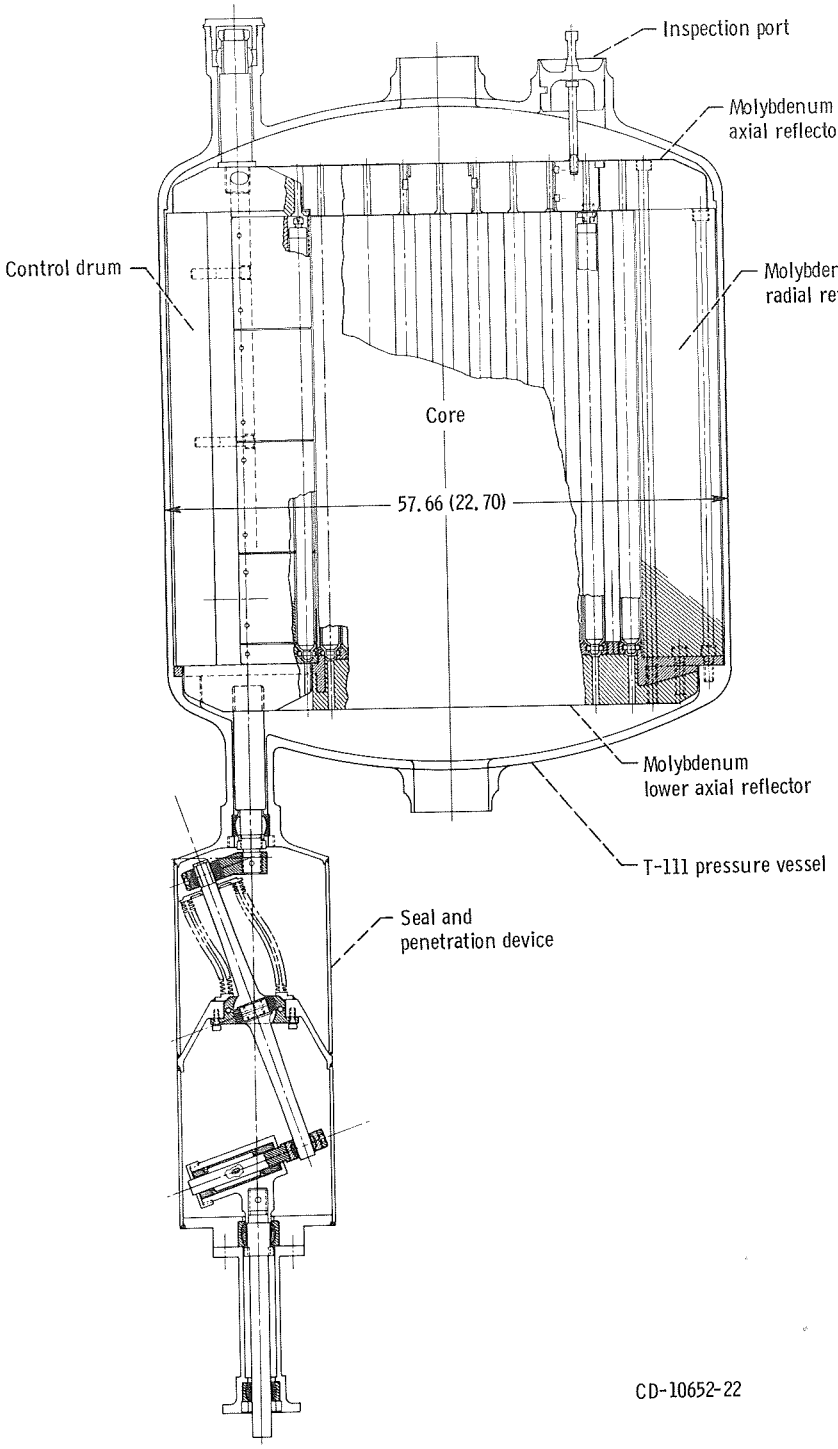

(b) Axial cross section.

Figure 2. - Concluded.

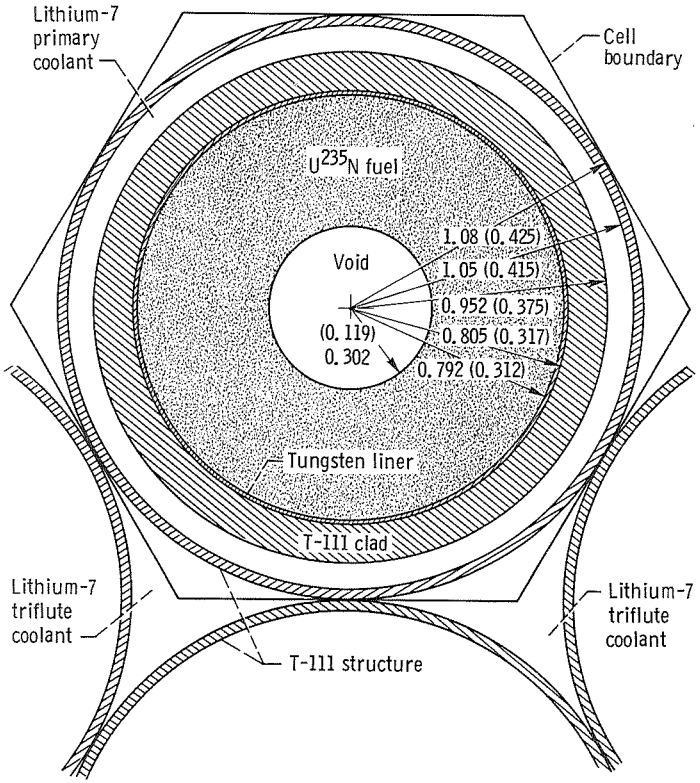

Figure 3. - Cell geometry (all dimensions are in centimeters (in.).)

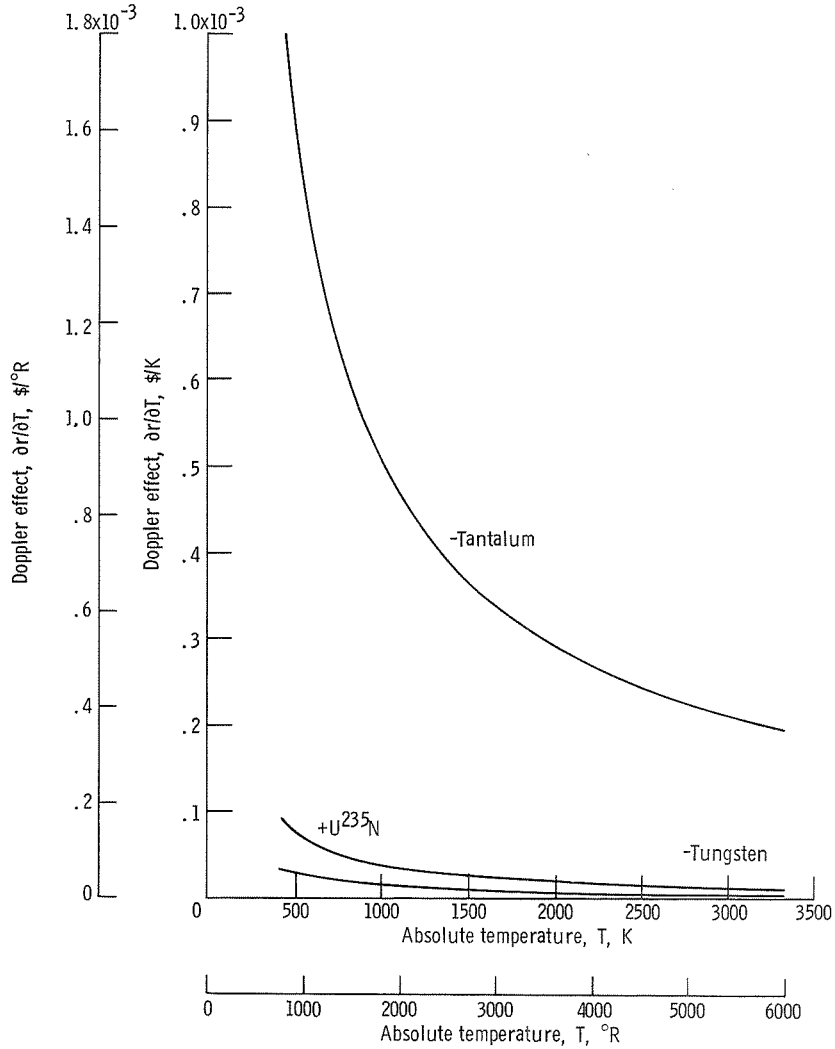

Figure 4. - Doppler reactivity coefficients.

also in the triflute channels in the honeycomb structure. The alloy TZM (Mo - 0.5 wt. % Ti - 0.08 wt. % Zr) is used as the reflectors. The pressure vessel and the poison vane in the control drums are made of T-111.

Time Constants

One measure of the thermodynamic response of a reactor to a transient power condition is the time constant (refs. 2 and 3)

$$\tau = \frac{\rho C_p V}{UA} \tag{1}$$

(Symbols are defined in appendix A.) Large time constants denote a sluggish reaction to a power transient. The relative thermodynamic response of different reactors may be compared by examining their respective time constants. Usually one is looking at the relation between the fuel and coolant regions. The time constants for these regions in some fast reactors are compared in table I. A larger time constant indicates a lower

TABLE I. - COMPARISON OF FUEL AND COOLANT TOME CONSTANTS

System	Time constant, sec	
	In fuel region	In coolant region
HCA	2.125	0.0437
Fermi[a]	.092	.044
EBR-I[a], MARK III	.75	.088

[a]Ref. 3.

ability to reject heat (or a greater capacity for retaining heat) during a transient. Because of the large time constant of the fuel, the thermodynamic response in the HCA will be slower than in other fast reactors, and the prompt Doppler and axial fuel expansion coefficients will take on a greater relative importance.

Reactivity Coefficients

Reactivity coefficients are divided into two classes: thermal expansion coefficients, which include density and geometry effects, and Doppler broadening coefficients. The thermal expansion coefficients, listed in table II, are assumed to be linear and have been calculated for the normal reactor operating range 460 to 1193 K (828° to 2150° R) (private communication from C. A. Whitmarsh of Lewis). The coolant expansion coefficient is divided between the primary and triflute regions according to the ratio of their volumes (2 to 1). The fuel and core expansion coefficients are assumed to depend on only one temperature - the clad temperature. This is a good assumption if the following conditions hold:

(1) The fuel is physically mated to the liner and clad.

(2) The fuel elements (fuel-liner-clad) have some clearance within the honeycomb structure.

The first condition is assumed to be met at the 461 K (830° R) initial temperature; above that temperature the expansion of the fuel, which has a coefficient of expansion larger than either the liner or the clad, maintains the condition. The second condition is due to clearances built into the honeycomb structure for fuel loading. In table II note

TABLE II. - THERMAL EXPANSION REACTIVITY COEFFICIENTS

Type	Thermal expansion reactivity coefficient, $\partial r/\partial T$			
	\$/K	$\$/^{\circ}R$	$(\delta k/k)/K$	$(\delta k/k)/^{\circ}R$
Axial fuel	-3.17×10^{-4}	-1.76×10^{-4}	-2.21×10^{-6}	-1.23×10^{-6}
Axial core	-.49	-.27	-.36	-.20
Radial core	-7.40	-4.11	-5.18	-2.88
Clad[a]	-11.06	-6.14	-7.75	-4.31
Coolant	-5.15	-2.86	-3.60	-2.00

[a]Clad values are sums of fuel and core values.

that the fuel and core expansion coefficients are combined and labeled as the clad expansion coefficient. Some calculations were also made with a clad expansion coefficient equal to -24×10^{-4} dollars per K (\$/K) (-13×10^{-4} $\$/^{\circ}R$). Even though the expected values are those listed in table II, the calculations based on the larger clad coefficient provides a measure of sensitivity of the reactor to a variation of that coefficient.

The reference set of Doppler coefficients are based on Brehm's formulas (ref. 4; see appendix B). The coefficients are nonlinear and, for reactivity r in dollars and T in degrees kelvin, take the form

$$\left.\frac{\partial r}{\partial T}\right|_{UN} = 0.128\ T^{-1} - 0.000679\ T^{-0.8} \tag{2a}$$

$$\left.\frac{\partial r}{\partial T}\right|_{W} = -0.135\ T^{-0.8} \tag{3a}$$

$$\left.\frac{\partial r}{\partial T}\right|_{Ta} = 0.414\ T^{-0.8} \tag{4a}$$

For T in ^{o}R units the coefficients are

$$\left.\frac{\partial r}{\partial T}\right|_{UN} = 0.128\ T^{-1} - 0.000604\ T^{-0.8} \tag{2b}$$

$$\left.\frac{\partial r}{\partial T}\right|_{W} = 0.0120\ T^{-0.8} \tag{3b}$$

$$\left.\frac{\partial r}{\partial T}\right|_{Ta} = -0.368\ T^{-0.8} \tag{4b}$$

The two UN terms are for U^{235} and U^{238}, respectively; the second term is neglected. Tungsten is found in three regions (liner, clad, and honeycomb), which are subjected to different temperatures during a power transient; hence, the contribution of the tungsten Doppler effect is mass weighted in each region (6:5:1 :: liner: clad: honeycomb). Likewise the tantalum Doppler effect is weighted in the clad and honeycomb regions in the ratio 30:7, respectively. Representative Doppler coefficients are given in table III. The Doppler coefficients of the important materials are plotted in figure 4. In figure 5 the

TABLE III. - DOPPLER COEFFICIENTS

Material	Doppler effect							
	\$/K		(δk/k)/K		\$/^{o}R		(δk/k)/^{o}R	
	Temperature, K				Temperature, ^{o}R			
	461	1111	461	1111	830	2000	830	2000
Uranium nitride	2.77×10^{-4}	1.15×10^{-4}	1.89×10^{-4}	0.77×10^{-4}	1.54×10^{-4}	0.64×10^{-4}	1.05×10^{-4}	0.43×10^{-4}
Tungsten	-.99	-.49	-.68	-.34	-.55	-.27	-.38	-.19
Tantalum	-30.62	-15.16	-20.83	-10.30	-17.01	-8.42	-11.57	-5.72

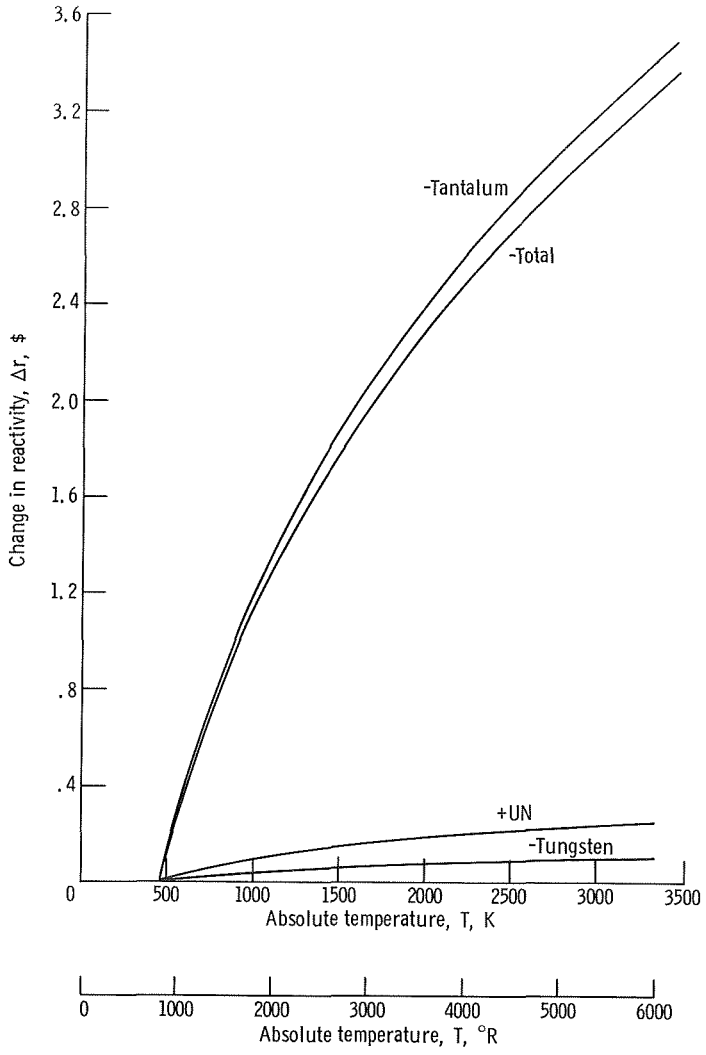

Figure 5. - Reactivity worths of Doppler effects. Base temperature, 461 K (830° R).

reactivity worth of each of these Doppler effects are plotted for a wide range of temperature changes based on an initial temperature of 461 K (830° R).

KINETICS WITH COOLANT

Model

The HCA with sliding reflector controls, as shown in figure 1, was modeled for the studies discussed in this section. This reactor is relatively small and has a fast spectrum (medium energy is 480 keV). Point reactor kinetics is assumed to suffice in

describing the kinetics. It is assumed that the core as a whole reacts as one average cell thermocynamically. The steady-state and transient results show that this is a reasonable assumption.

AIROS accepts a nodal model of the reactor system with thermal feedbacks. For the point reactor studies, an average cell is chosen to represent the core. Each material component in the cell is represented as well as each region of the reactor. The resulting nodal network is shown in figure 6. Reactivity feedback effects are connected directly to

Cell

Fuel	Liner	Clad	Coolant primary	Honeycomb structure	Coolant triflute
$U^{235}N$	W	T-111	Li^7	T-111	Li^7
U^{235} Dop	W Dop	W, Ta Dop	Li^7 Dop	W, Ta Dop	Li^7 Dop
(UN axial Exp)		Clad Exp		(Core radial Exp)	
1	2	3	4	5	6

Reactor

Core	Coolant	Pressure vessel	Reflectors			Shield	Sink
	Li^7	T-III	92 vol. % Mo (rest void)	92 vol. % Mo (rest void)	85 vol. % Mo 15 vol. % Li^7	75 vol. % LiH 15 vol. % Mo 10 vol. % Li^7	Inert gas
	(Core radial Exp)						
I	II	III	IV	V	VI	VII	VIII

Figure 6. - Nodal model for HCA with sliding reflector control. Doppler (Dop) and thermal expansion (Exp) reactivity effects are placed in the node whose temperature controls the effect. Those in parentheses are used only in special cases as explained in section Results. Numbers at bottom are node numbers used in feedback equations (7) to (10).

the material and region responsible for them, and the effect of both temperature and transport delay can be observed correctly.

Two reactivity effects are represented: Doppler broadening and thermal expansion. Thermal expansion includes geometry and density effects. Doppler broadening in U^{235}, W, and Ta is considered; it is neglected in U^{238} because of the relatively insiginficant amount involved. It is a prompt effect, that is, it is directly affected by the temperature of the material involved.

If a gap exists between the fuel and the liner, the fuel expands freely in both radial and axial directions. If no gap exists between the liner and the fuel, the radial portion of the fuel expansion is constrained by the radial expansion of clad since UN has a greater

coefficient of expansion than T-111. Hence, to be conservative, the expansion of the fuel was assumed to be the same as the clad. In this case the axial expansion is somewhat more complicated. The fuel is constrained at its outer surface to a degree determined by the friction involved at the contact surface, so that axial thermal expansion produces a bulge at both ends (see fig. 7). The axial expansion coefficient is thus divided between

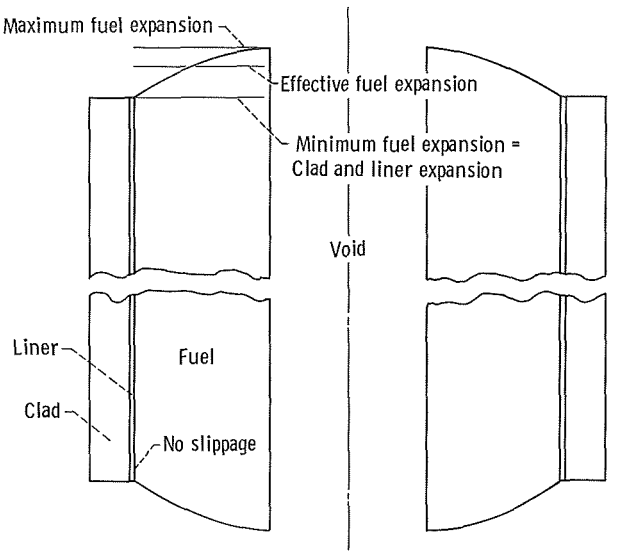

Figure 7. - Axial fuel expansion by bulging.

the prompt portion in the fuel region due to the bulging and the delayed portion in the clad due to axial expansion in the clad. The model used in the calculations is conservative in this respect because all axial expansion is normally tied in with the clad expansion.

The reactivity effect of radial core expansion is chiefly the increase in core radius due to radial fuel displacement. For fast transients, it is assumed that the temperature rises within each cell before much heat is transmitted out of the core. In the cell, the fuel-liner-clad annulus expands into the coolant channel to effect the increase in core radius. Thus the radial core expansion effect is also dependent on the clad region.

Equations

The reactor dynamics equations with feedback equations have been put into a general code for digital computers. The AIROS (ref. 1) code was developed for fast reactor power dynamics. It solves the time-dependent one-group neutron diffusion equation with up to 15 precursor groups (as given by eqs. (5) and (6)).

$$\frac{dN(t)}{dt} = \frac{\beta}{\ell}\left[r(t) - 1\right] N(t) + \sum_i \lambda_i C_i(t) \tag{5}$$

$$\frac{dC_i(t)}{dt} = \frac{\beta f_i}{\ell} N(t) - \lambda_i C_i(t) \tag{6}$$

The reactivity equation

$$r(t) = r(o) + \mathrm{Min}(\gamma_1 t, \gamma_2) + \sum_j B_j \delta T_j(t) \tag{7}$$

allows a variety of ramp inputs and reactivity feedbacks. The input function $\mathrm{Min}(\gamma_1 t, \gamma_2)$ describes a ramp with initial slope γ_1 and a break at γ_2, after which the reactivity input is held constant at γ_2. The reactivity feedback effects are described by the terms under the summation sign. The B_j are constants, and the $\delta T_j(t)$ have various forms of temperature dependence. The reactivity coefficients are assumed to take the form

$$\left.\frac{dr}{dT}\right|_{\text{Feedback j}} = \frac{d\left[B_j \delta T_j(t)\right]}{dT} = B_j T_j^{-a}(t) \tag{8}$$

which may be linear (a = 0) for thermal expansion effects or nonlinear for Doppler effects. The B_j constants for the expansion effects are found in table II. The B_j and a for the Doppler effects are found in equations (2) to (4).

Reactivity feedbacks are affected by the temperature relations in the nodes (1 to 6 for the cell, I to VII for the HCA system, as in fig. 6), as governed by the equations

$$\frac{dT_1(t)}{dt} = \frac{H_1}{\left(\rho C_p V\right)_1} N(t) - \frac{(UA)_{12}}{\left(\rho C_p V\right)_1}(T_1 - T_2) \tag{9}$$

$$\frac{dT_i(t)}{dt} = \frac{(UA)_{i-1,i}}{\left(\rho C_p V\right)_i}(T_{i-1} - T_i) - \frac{(UA)_{i,i+1}}{\left(\rho C_p V\right)_i}(T_i - T_{i+1})$$

where i = 2 to 6 and II to VII. The sink temperature is considered to be constant at 461 K (830° R).

Results

Steady state. - The steady-state calculations were performed to help verify the assumption that a single average cell is a sufficient model of the heat transfer in the core. The radial temperature distributions of the HCA for a range of average core temperatures are shown in figure 8. Since the difference in the temperatures over the core are not large, a single node is sufficient to represent the temperature of the core as a whole.

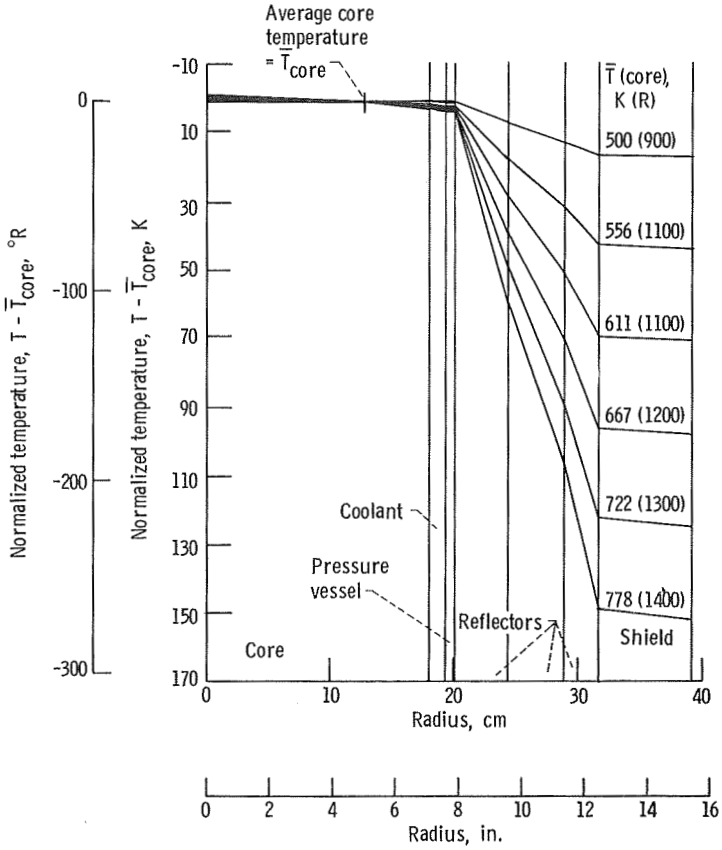

Figure 8. - Steady-state temperature distributions. Sink temperature, 461 K (830° R).

A sink temperature of 461 K (83^{o} R) must be maintained to keep lithium in a molten state. At this sink temperature higher average core temperatures may be obtained by operating at higher power levels, as shown in figure 9. Figure 9 also shows equivalent neutron flux and neutron densities. The average neutron velocity is 9.62×10^{8} centimeters per second (cm/sec), and a 1 n/cm^{3} density is equivalent to 20 watts of thermal power.

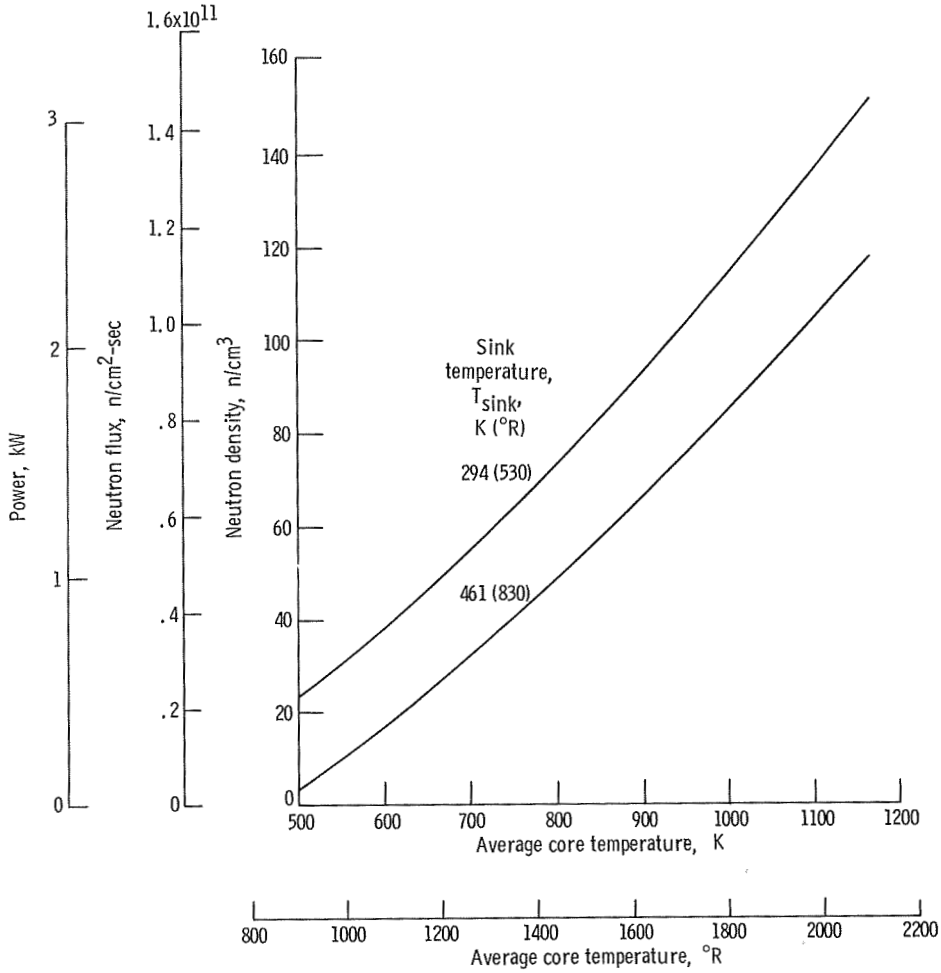

Figure 9. - Power and neutron flux and density at various steady-state conditions.

Kinetics of reference model. - The following results deal with the HCA in a startup condition, which is potentially the most dangerous operating condition. To be conservative the fuel is assumed to be initially mated to the liner and clad. Therefore, throughout the transients the fuel expands only as the clad expands. Bulging at the fuel element ends is neglected. Hence, the fuel expansion reactivity feedback becomes a delayed effect and is governed by the clad expansion. The Doppler reactivity effect is positive in the fuel region.

A ramp reactivity input was used in this study. A usual result of a ramp input under safe startup conditions is a fuel temperature curve that reaches its peak gradually as shown in the curve of figure 10 for the 92-cents (¢) case. As the ramp approaches less safe conditions, an initial peak will form on the temperature curve like the one shown in figure 10 for the case of 98¢, and it is the magnitude of this initial peak which determines the limits for safe operation.

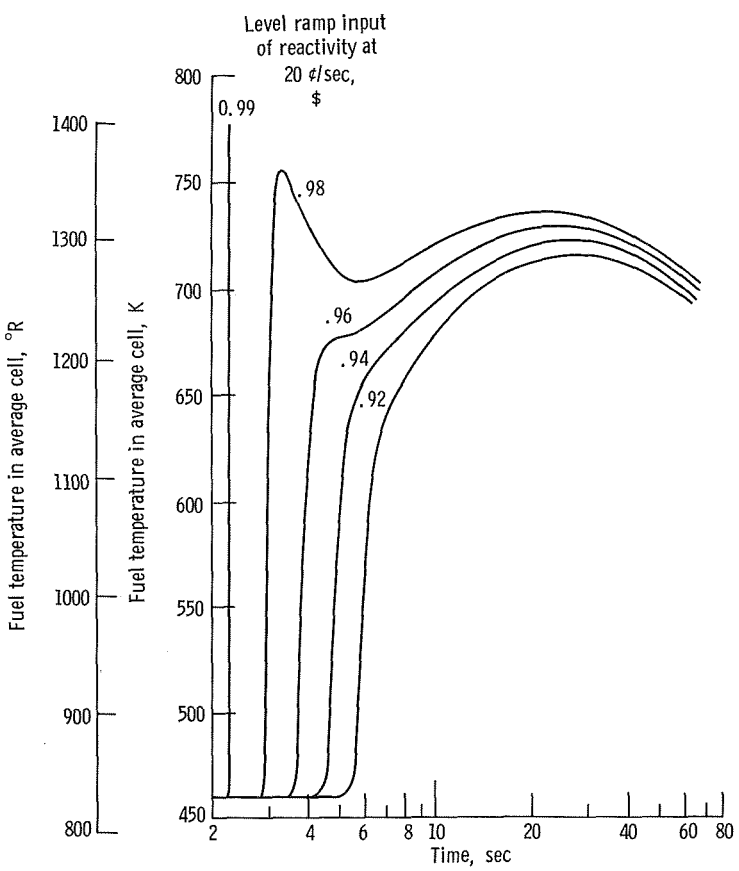

Figure 10. - Initial peak formation in fuel temperature transients. Neutron density, 1 cm^3; temperature, 461 K (830° R).

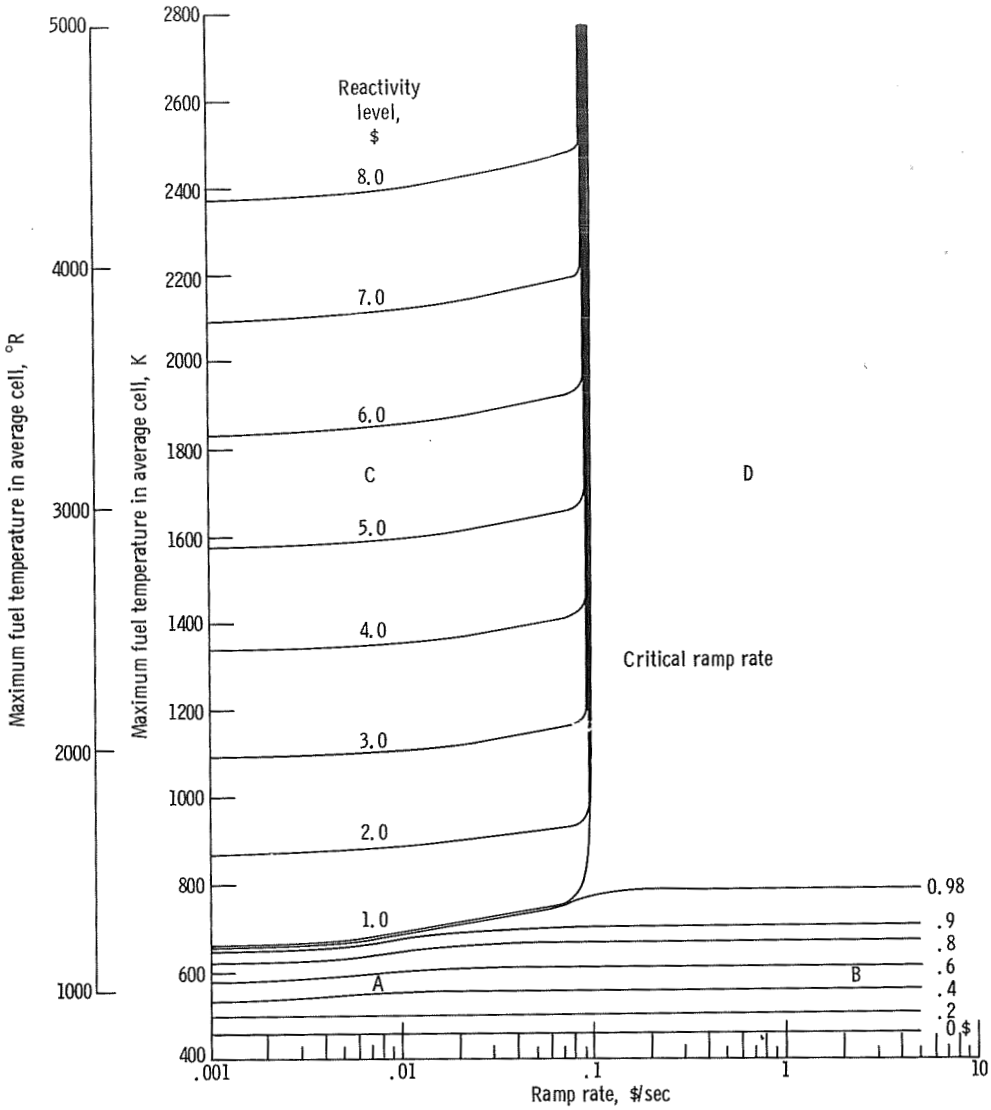

Figure 11. - Sensitivity of fuel temperature transients to ramp reactivity inputs in HCA with coolant. Expansion coefficients: clad, -24×10^{-4} \$/K (-13×10^{-4} \$/°R); coolant, -5×10^{-4} \$/K (-3×10^{-4} \$/°R). See table III for Doppler coefficients. Startup from delayed critical with all temperatures at 461 K (830° R); initial power, 20 watts.

The results of a parametric study of the effects of ramp rate and ramp level on fuel temperature are shown in figure 11. Four distinct regions are labeled in the figure in order of decreasing safety:

(A) Transition region, <9 cents per second (¢/sec) and ≤98 ¢

(B) Step-input region, >9 ¢/sec and ≤98 ¢

(C) Large-input region, <9 ¢/sec and >98 ¢

(D) Forbidden region, >9 ¢/sec and >98 ¢

Some typical transients of regions A and B are shown in figure 12. In these regions the initial power peaks shown in figure 12(a) are not reflected in the temperature tran-

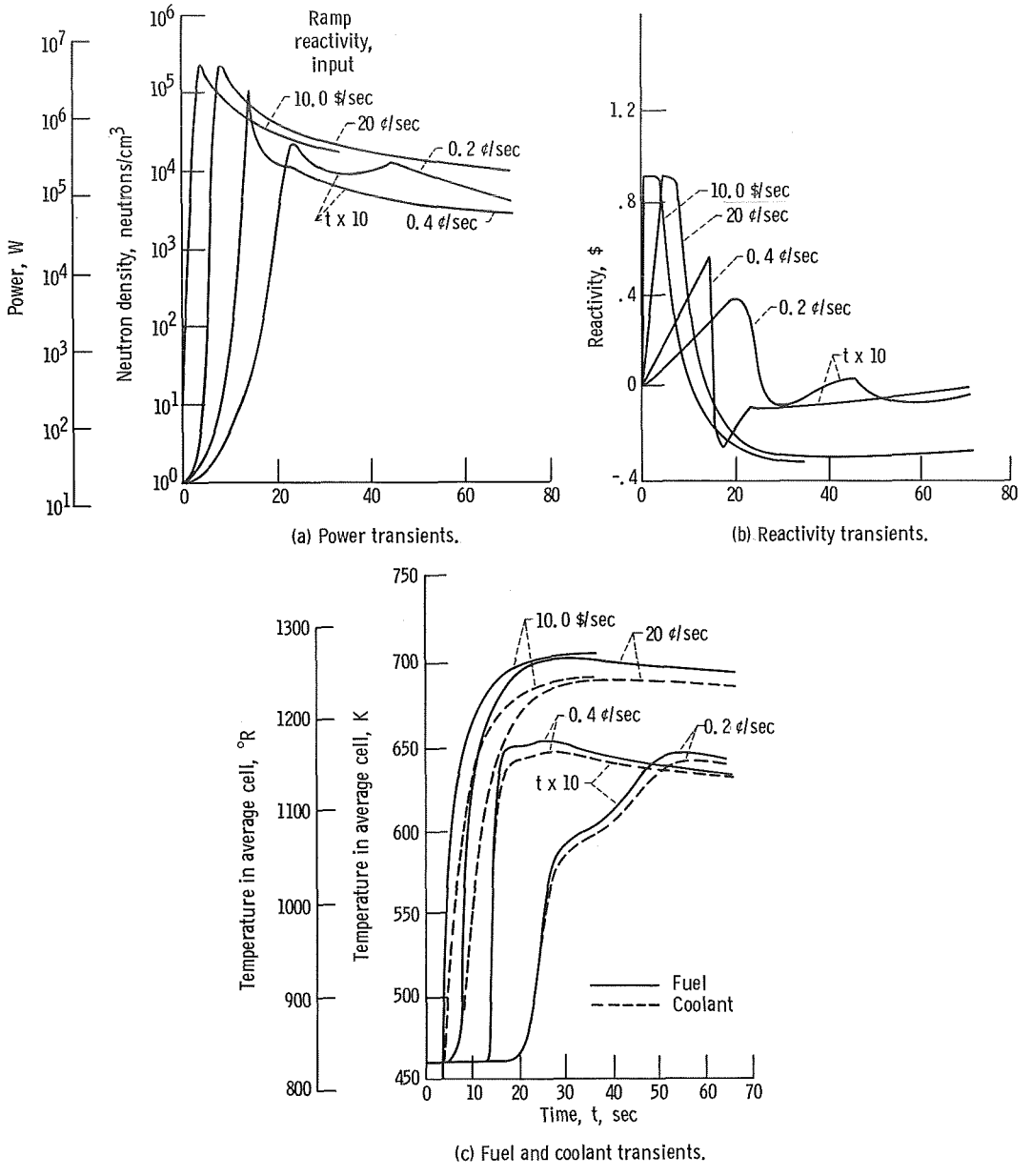

Figure 12. - Transients for some ramp reactivity inputs with 90-cent level, HCA with coolant. Expansion coefficients: clad, -24×10^{-4} \$/K (-13×10^{-4} \$/°R); coolant, -5×10^{-4} \$/K (-3×10^{-4} \$/°R). See table III for Doppler coefficients.

sients in figure 12(c). The start of temperature rise is delayed by the low startup power. The power will increase by about five orders of magnitude before enough heat is produced to significantly change any temperatures. Above 0.2 dollar per second (\$/sec), the maximum value of the temperature transients are unchanged by any further increase of the ramp rate; in this sense the ramp inputs effectively become step inputs. Below 0.2 \$/sec, there is a transition zone in which the maximum fuel temperature transient becomes dependent on the ramp rate.

In regions A and C, which have rate-dependent temperature maximums, much of the effect of temperature feedbacks has taken place before all of the reactivity has been inserted, so that the total reactivity never reaches the input reactivity level. Although the input reactivities in region C are ≥ 1 \$ the temperature feedbacks react fast enough to prevent the HCA from reaching prompt criticality (see fig. 13). At a critical insertion rate of about 9 ¢/sec this mechanism breaks down, and the reactor becomes

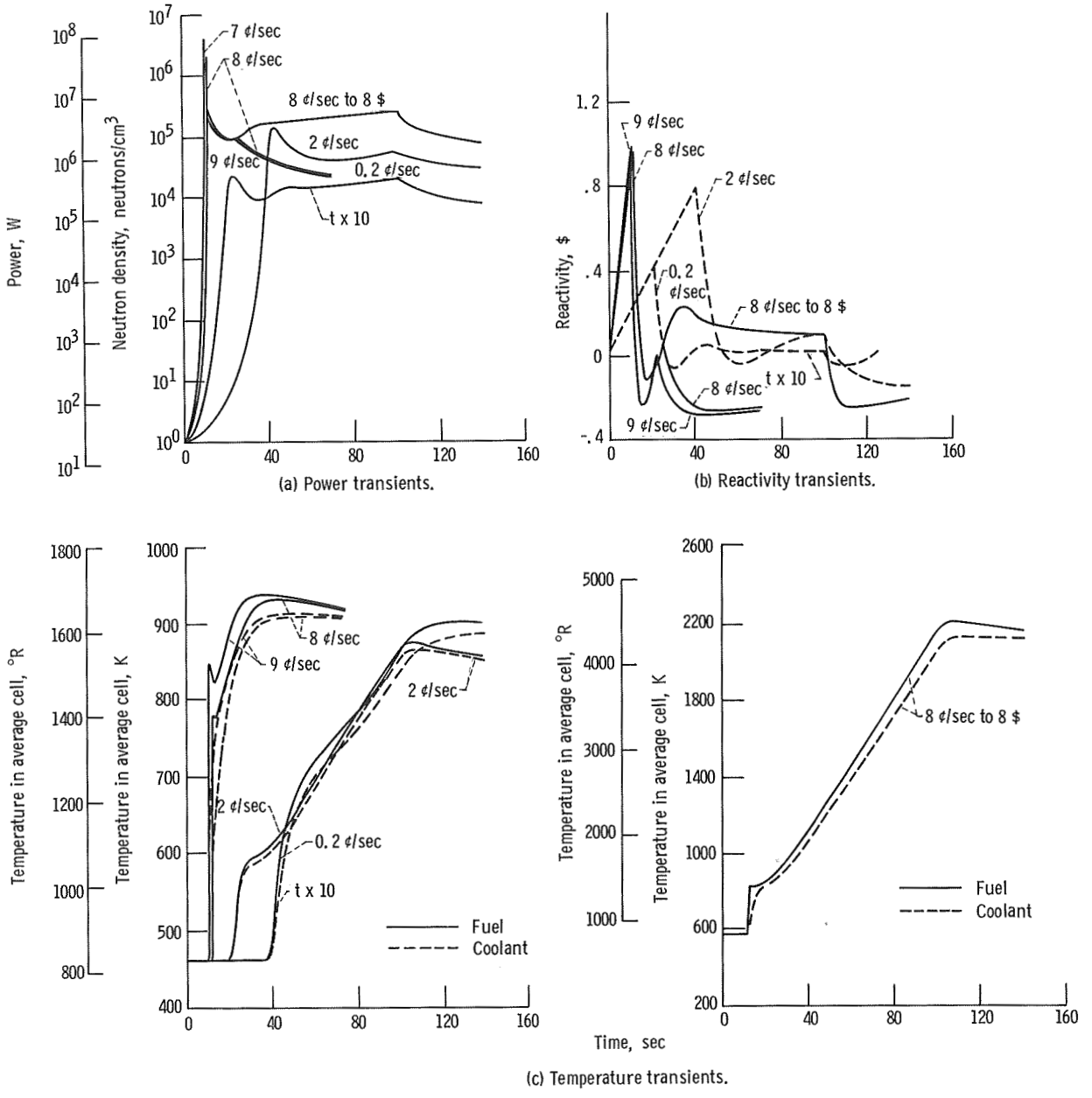

Figure 13. - Transients for some ramp reactivity inputs with 2- and 8-dollar levels (level is 2$ unless otherwise specified). HCA with coolant. Expansion coefficients; clad, -24×10^{-4} \$/K (-13×10^{-4} \$/°R); coolant, -5×10^{-4} \$/K (-3×10^{-4} \$/°R). See table III for Doppler coefficients.

super prompt critical, which results in a catastrophic excursion. The cause of the critical ramp rate is the time delay between the small prompt positive fuel reactivity effect and the large delayed negative reactivity effect in the other materials. The 8- and 9-¢/sec curves in figure 13(b) have reactivity peaks close to 1 $. As the input reactivity approaches 1 $ the prompt positive Doppler feedback will carry the reactivity over prompt critical if there is sufficient delay in the negative feedback. The HCA there is a delay of about 11 seconds, which is critical to whether the overall reactivity feedback will add to or subtract from the input reactivity ramp. The initial peaking of the neutron density and the temperatures at 8 and 9 ¢/sec provides a warning that a danger point is being approached. Far away from the critical insertion rate peaking is no longer in evidence.

All ramp speeds are allowable for safe operation at reactivity insertions up to about 90 ¢. Theoretically, 98 ¢ is also safe except that it is dangerously close to 99 ¢, which results in full excursions (extremely high temperatures resulting in gross fuel meltdown and coolant vaporization) at ramp speeds greater than 9 ¢/sec. To handle reactivity insertions of 1.0 $ or more, the ramp rate must be limited to less than 9 ¢/sec to prevent a full excursion from occurring. The full insertion of one fuel drum (180^{o} of rotation) represents 1.43 percent $\delta k/k$ or 2.47 $ of reactivity. Thus, at 1.37 cents per degree ($¢/^{o}$), the maximum drum rotation rate must be limited to 6.5 degrees per second. At this rate it would take at least 28 seconds to rotate a drum in.

Uranium nitride fuel melts at 3120 K (5620^{o} R) (ref. 5). For insertion rates close to 10 ¢/sec, the maximum fuel temperature in the hottest fuel channel is about 780 K (1400^{o} R) higher than the average fuel temperature (ref. 6). Therefore, the limiting average fuel temperature is set at ~2300 K (4200^{o} R), below which no fuel melting will occur in the HCA. At the beginning of life the total excess reactivity available may be as much as 5 percent $\delta k/k$, or 7 $. As shown in figure 11, all 7 $ could be inserted without melting the fuel as long as it is inserted at less than 9 ¢/sec. However, the reactivity coefficients expected in the HCA are smaller than these in figure 11. It will be shown in the next section that the entire 7 $ cannot be inserted without fuel melting, when the smaller coefficients are considered.

The value of each feedback in pulling the input reactivity down and keeping the total reactivity less than a dollar is illustrated in figure 14. The shape of the expansion curves are proportional to the temperature curves in figure 13(c) for the respective regions. Although the input reactivity reaches a level of 2 $, the total reactivity peaks at less than 0.4 $, having a safety margin of 0.6 $. The Doppler effect in the liner and structure regions is due almost entirely to tantalum (1.64 percent due to tungsten). The major effort in reducing the reactivity is shared nearly equally by the Doppler effect in the cladding and the expansion effect of the fuel. The Doppler effect shown here is then due to Brehm's formulas, and the actual value in the HCA is expected to be lower.

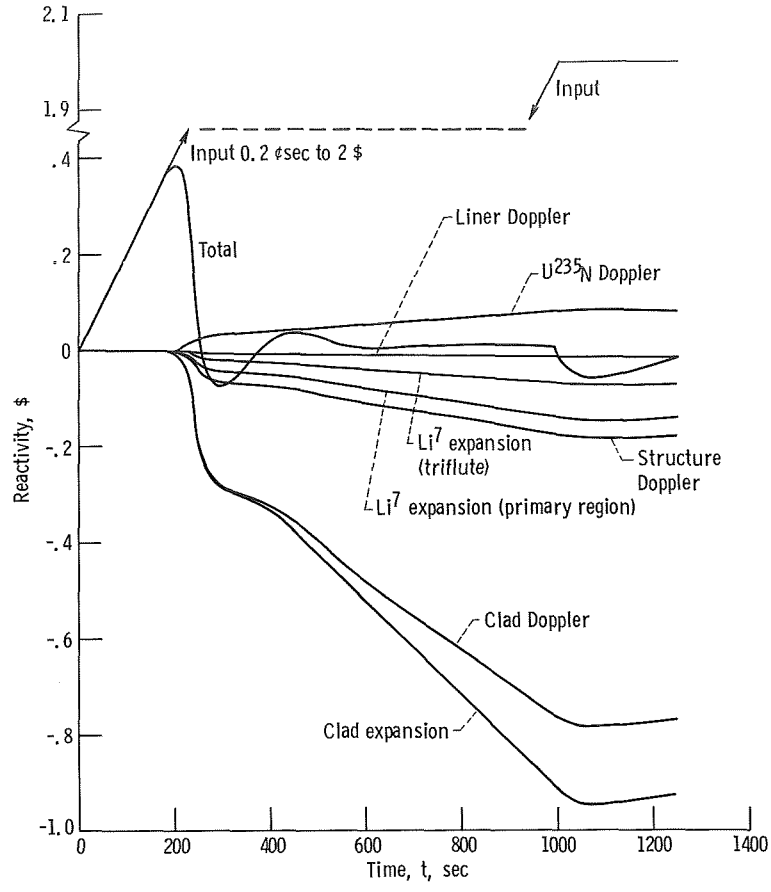

Figure 14. - Component breakdown of reactivity transient. Expansion coefficients: clad, -24×10^{-4} \$/K (-13×10^{-4} \$/°R); coolant, -5×10^{-4} \$/K (-3×10^{-4} \$/°R). See table III for Doppler coefficients.

Figure 15 shows that different initial neutron densities (powers) have little effect on the peak neutron densities and temperatures as long as the initial neutron densities do not stray far from those expected at startup. For the range $N(0) = 1$ to 1000 n/cm^3 (20 to 20 000 W) the average fuel temperature will always reach the same maximum, and the neutron density peak will vary no more than 8.5 percent. For input reactivity ramps reaching the same absolute reactivity level, calculations in the 0- to 3-\$ range of initial shutdown reactivity show that the shutdown reactivity has no effect on the maximum values of temperature or neutron density. The time interval for reaching the maximum is increased, however, due to the longer ramp required to reach the same absolute reactivity level. For example, introducing reactivity to the 1-\$ level at the rate of 20 ¢/sec from a 2-\$ shutdown level takes 10 seconds longer than from delayed critical. This accounts for the time lag in reaching the maximum power and temperature. The maximum average fuel temperature increases 0.63 K (1.13° R) per degree rise in the initial HCA temperature. Factors of 0.5 and 2 applied to the lifetime $\ell = 5 \times 10^{-8}$ sec and to the delayed

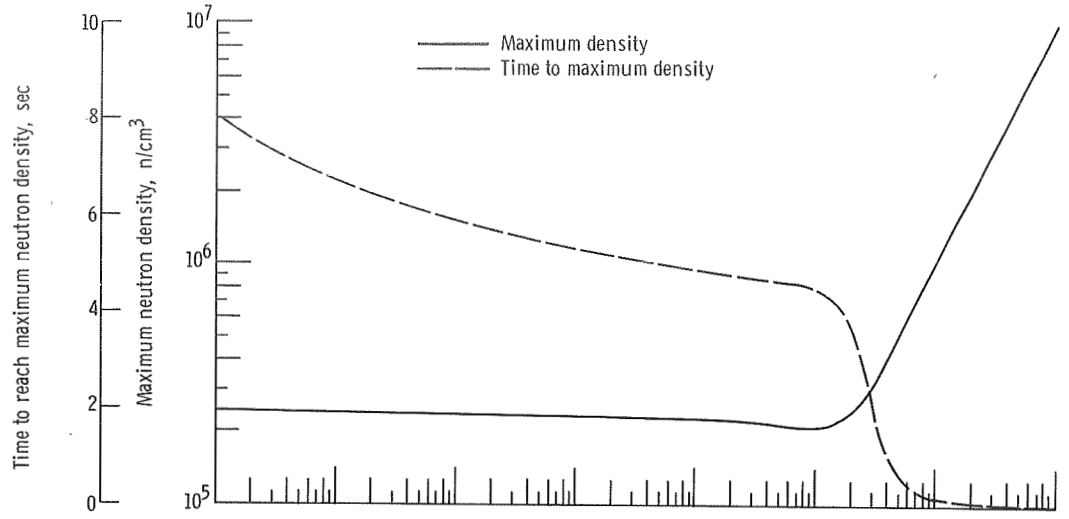

(a) Effect on power transients.

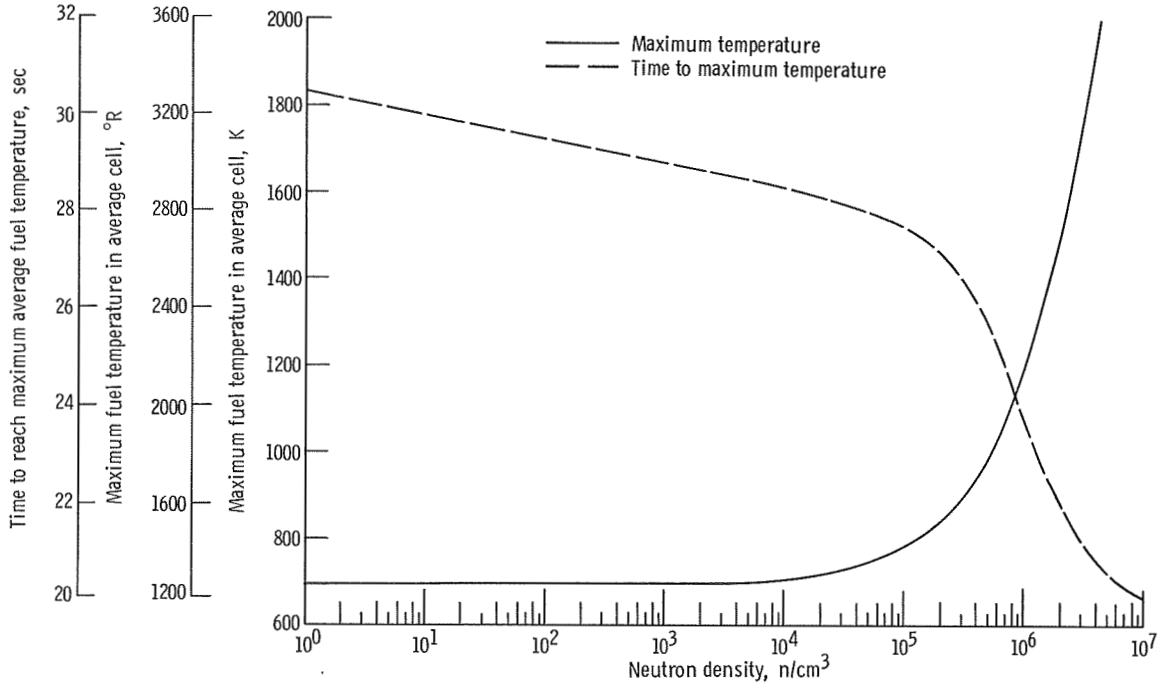

(b) Effect on fuel temperature transients.

Figure 15. - Effect of initial power level on transient. Reactivity input, 20 ¢/sec to 90 ¢; all initial temperatures, 461 K (830° R).

neutron fraction $\beta = 0.0068$ produced no effect on the results of the 20 ¢/sec to 90 ¢ ramp input.

Variations on the reference model. - The knowledge and experience with fast reactor reactivity coefficients is insufficient to predict reliably and accurately the reactivity effects of a particular combination of materials and geometry. Hence, the initial kinetic

studies of the HCA needs to be parametric and broad in scope.

Some information is gained in comparing this system with other fast reactors already in operation. A comparison of expansion and Doppler reactivity coefficients is presented in table IV. The magnitude of the HCA coefficients are largest; this tends to make the HCA a relatively safer system to operate. However, the heat-transfer response also plays a large role, and it is the interaction of these factors which determines the overall safety of the system.

TABLE IV. - COMPARISON OF REACTIVITY COEFFICIENTS

System	Expansion coefficient		Doppler coefficient	
	$(\delta k/k)/K$	$(\delta k/k)/^{o}R$	$(\delta k/k)/K$	$(\delta k/k)/^{o}R$
HCA	-11.36×10^{-6}	-6.31×10^{-6}	-12.91×10^{-6}	[b] -7.17×10^{-6}
FERMI[a]	-6.16	-3.42	-2.54	-1.41
SEFOR[a]	-4.81	-2.67	-6.39	-3.55
EBR-II[a]	-3.60	-2.00	-.40	-.22

[a]Data from ref. 7.

[b]Averaged over range 461 to 1222 K (830^{o} to 2200^{o} R).

The best estimates of the thermal expansion and Doppler coefficients of reactivity were used in the reference model. In the following sections some variations on this model are investigated. These studies are divided into three parts. The first is a parametric study of smaller reactivity feedback effects on the fuel temperature. These effects include changes in the magnitude of the coefficients and changes in the distribution of fuel expansion coefficient between the fuel and clad regions due to fuel bulging. The second is a study of different reactivity coefficients on the maximum safe reactivity input level. The third is a search for a value of the Doppler coefficient for which the critical ramp rate (the rate above which reactivity inputs greater than 1 $ are forbidden) does not exist.

Reactivity coefficient magnitude: The effects on maximum fuel temperature of changing the values of reactivity coefficients have been studied in the case of a 20 ¢/sec to 90 ¢ reactivity ramp input, and the results are given in figure 16. In figure 16(a) the effects of decreasing only the expansion coefficients are shown. Each curve is the result of changing the expansion coefficient(s) indicated on the curve and holding the other reactivity coefficients constant. Keeping the expansion coefficients constant and varying the Doppler coefficients results in the curves shown in figure 16(c). In this case the curve labeled All refers to changing each of the Ta, W, and UN Dopplers coefficients by the same ratio. It is the combination of smaller expansion and Doppler reactivity coeffi-

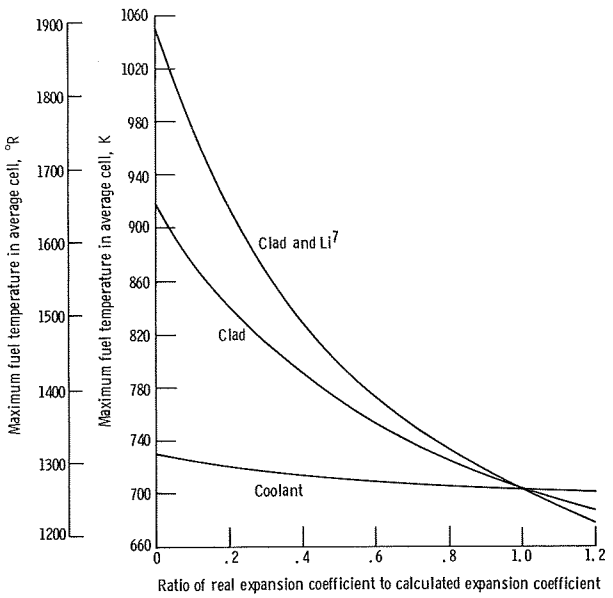

(a) Effect of thermal expansion coefficient.

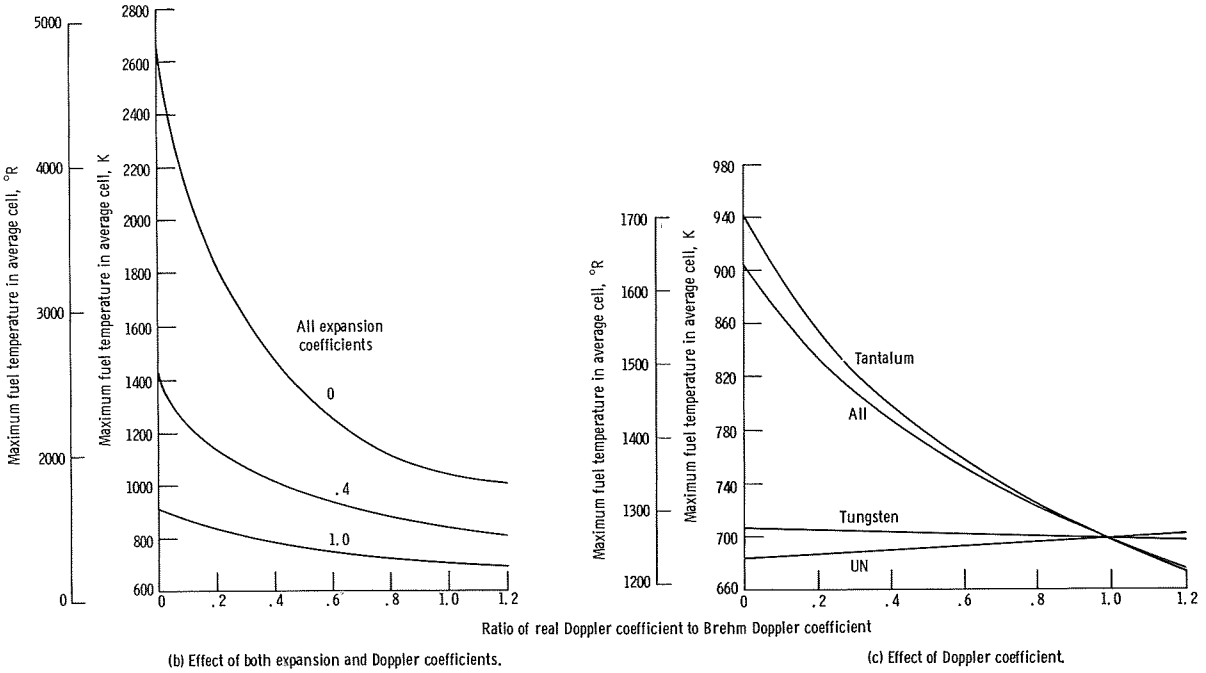

(b) Effect of both expansion and Doppler coefficients.

(c) Effect of Doppler coefficient.

Figure 16. - Effect of variations in reactivity coefficients on fuel temperature transient. Reactivity input rate, 20 ¢/sec to 90 ¢; initial power, 20.5 watts; initial temperature, 461 K (830° R). Expansion coefficients: clad, -24×10^{-4} \$/K (-13×10^{-4} \$/°R); coolant, -5×10^{-4} \$/K (-3×10^{-4} \$/°R). See table III for Doppler coefficients.

cients which leads to excessively large deviations from the base case, as shown in figure 16(b).

Since UN has a greater coefficient of expansion than T-111, the expansion of UN is controlled by T-111 expansion after the fuel mates with the clad. The reactor is designed

such that mating takes place at 461 K (830° R). When the fuel has expanded against the line in this fashion, the stresses are such that no axial slippage of the UN is allowed. However, UN axial expansion may still take place by the bulging of fuel at the ends of the fuel element (fig. 7). The prompt positive Doppler coefficient in the fuel is partially overridden by the prompt negative axial coefficient when bulging occurs. In figure 17 it

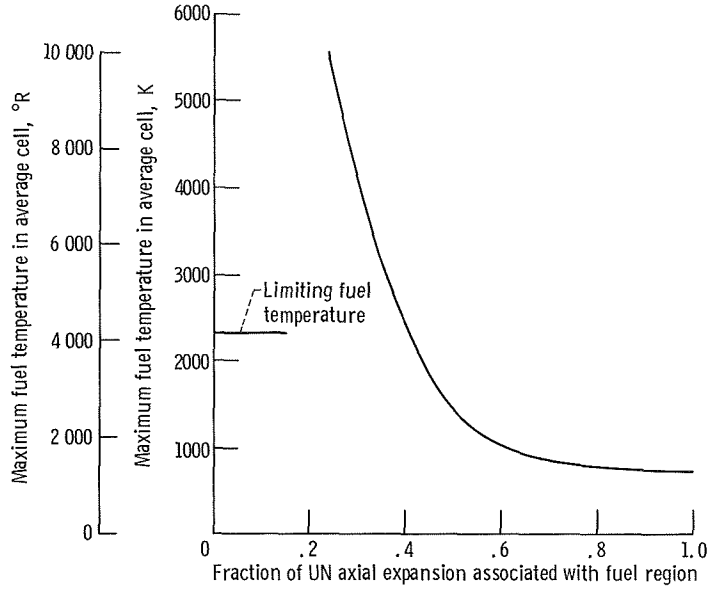

Figure 17. - Effect of UN axial expansion on fuel temperature transient. Reactivity input, 20 ¢/sec to 1$.

is shown that at least 40 percent of the UN axial expansion must effectively take place in the bulging in order to make a fast 1 $ insertion safe. When about 85 percent of the UN axial expansion is available in the fuel region, the overall reactivity coefficient in the fuel becomes negative, and the system no longer has a critical ramp rate (i.e., insertions greater than 1 $ can be taken at any rate). In this case the HCA is safe for all insertions of reactivity contained in the control devices, which is about 7 $.

Reactivity insertion limit: The size of the reactivity coefficients has a considerable effect on the maximum reactivity level that can be inserted at less than 9 ¢/sec and not melt any fuel. The results of the behavior in the region near the 2300 K (4200° R) limiting fuel temperature are shown in figure 18. Curve A represents the largest coefficient considered and is the same case shown in figure 11 (region C). If the reactivity coefficients in the HCA are 11×10^{-4} \$/K (6×10^{-4} \$/°R) for the clad expansion and the Doppler is 0.2 of that predicted by Brehm's formulas, then the input reactivity must be limited to about 3.1 $ (curve E) rather than the 7.5 $ limit shown in figure 11. Whether the radial core expansion is affected by the clad temperature (curve D) or by the temperature

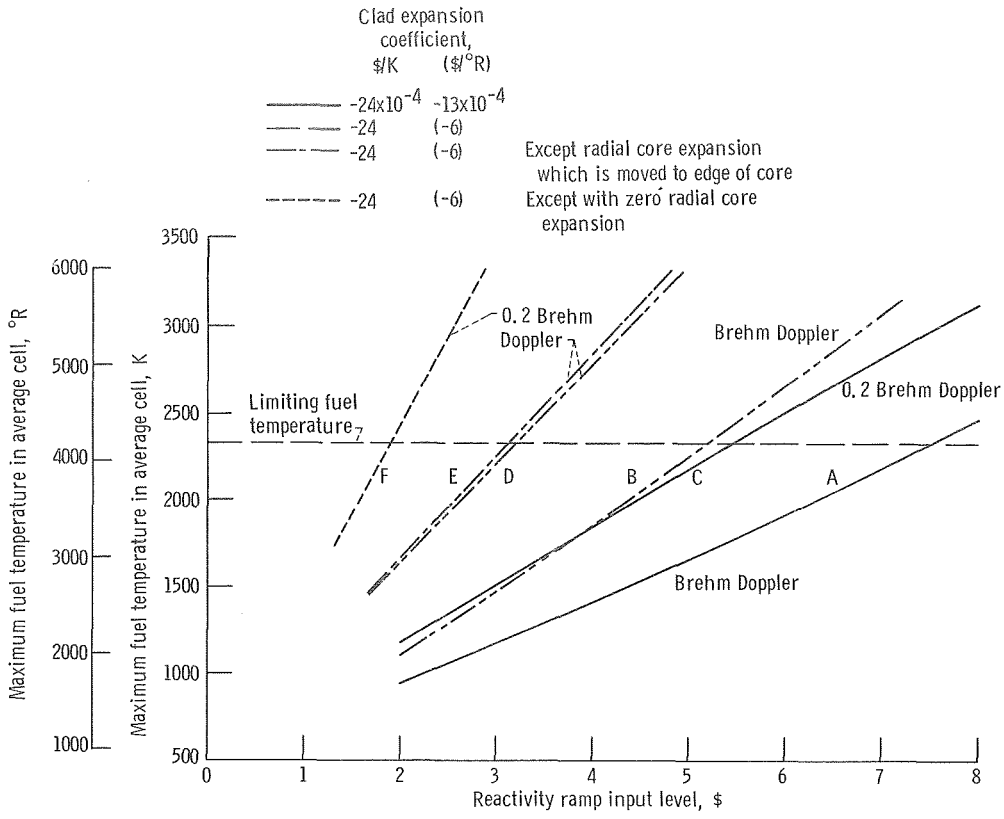

Figure 18. - Effect of lower Doppler coefficient on maximum safe reactivity input level. Reactivity input rate, 5 ¢/sec.

of the coolant just outside the core (curve E) has little effect (~10 ¢) on the safe reactivity input level. This follows from the fact that the lithium coolant is such a good heat transmitter. The magnitude of radial core expansion effect is important, however. If the core does not expand, the reactivity insertion limit would be below 2 $. Since one control drum is worth about 2.5 $, steps would have to be taken to insure that the fuel would not melt. Either failsafe interlocks would have to be provided to prevent the full insertion of a control drum, or the design would have to be changed to accommodate a larger number of drums, each worth less than 2 $.

Critical ramp rate: Using Brehm's formulas for the Doppler coefficients can be taken only as an approximation. The true values for the HCA can only be found by actual measurement. Figure 19 shows the effect that a wide discrepancy between the real and calculated Doppler coefficients would have.

For a 1-$ insertion, it is possible to remove critical ramp rate (i.e., the rate for which an excursion will occur) if the Doppler is decreased sufficiently, as shown in figure 19. In the plateau region above 40 ¢/sec the reactor sees a ramp input as essentially a step input; the feedback reaction times are much longer than the reactivity input time. In the region between 5 ¢/sec and 40 ¢ there is a transition region in which the temper-

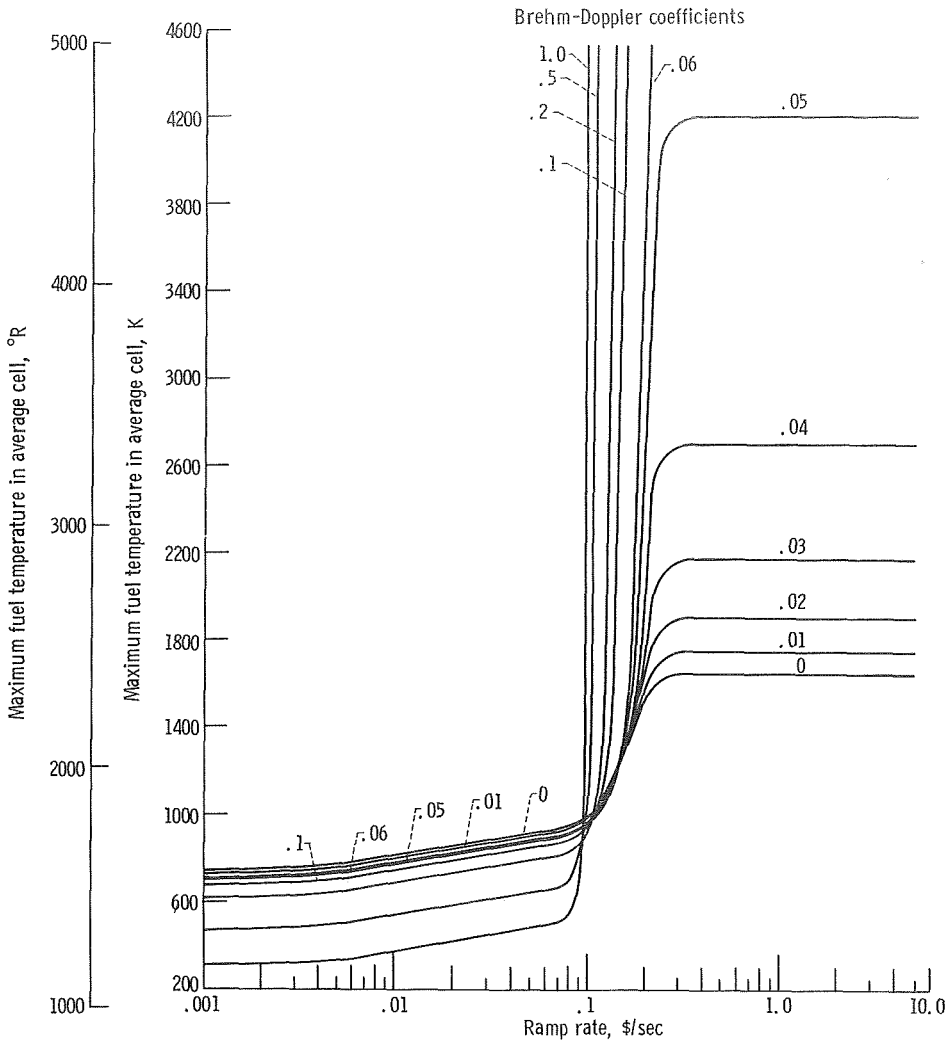

Figure 19. - Effect of decreasing all Doppler reactivity coefficients on fuel temperature transients. Startup from delayed critical with all temperatures at 461 K (830° R). Initial power, 20.5 watts. Expansion coefficients; clad, -24×10^{-4} \$/K (-13×10^{-4} \$/°R); coolant, -5×10^{-4} \$/K (-3×10^{-4} \$/°R). See table III for Doppler coefficients.

ature curves take on an initial peak in additional to the more gradually rising maximum (similar to those in fig. 10). As this peak becomes more fully developed for increasing rates of reactivity input, the gradually rising maximum is lost in the tail of the initial peak. This is more clearly understood by comparing the graphs of some transients for small Doppler coefficients, as shown in figure 20, with the transients shown in figures 10, 12, and 13.

Even if Brehm's formulas are sufficiently inaccurate in this case so that the HCA Doppler coefficients are in actuality closer to the values for the Fermi reactor, the 0.2-Brehm-Doppler curve in figure 19 coefficient would apply. Thus, the HCA is still expected to have a critical ramp rate in the neighborhood of 9 ¢/sec, which may be slightly on the conservative side.

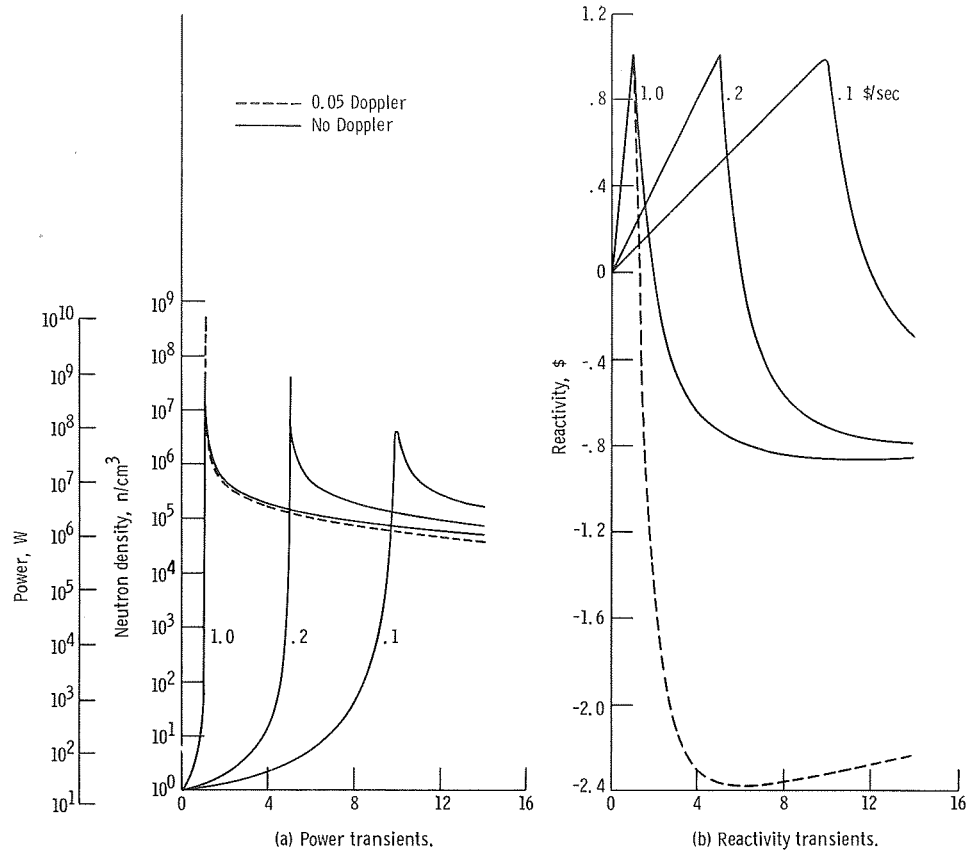

(a) Power transients.

(b) Reactivity transients.

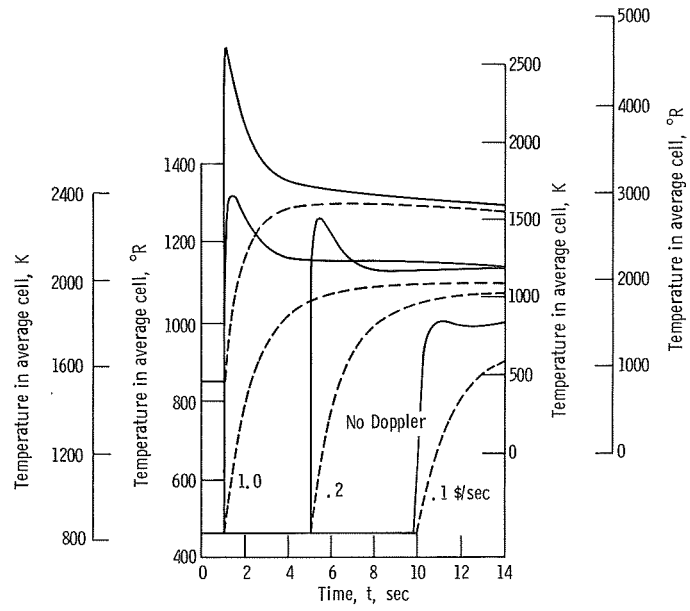

(c) Fuel and coolant temperature transients.

Figure 20. - Transients for 0 and 0.05 times Brehm-Doppler coefficient. Ramp level, 1 dollar; initial temperature, 431 K (830° R); initial density, 1 neutron per cubic centimeter.

KINETICS WITHOUT COOLANT

Model

The model (fig. 2) for the studies discussed in this chapter is the HCA with control drums. Modeling of the core is complicated by the heat-transfer treatment (see fig. 21(a)). Heat produced in the fuel regions is transmitted to the outer surface of the clad by conduction and across the empty coolant channel to the structure by radiation. Heat transfer from an individual cell to the outside of the core is complicated by the array of

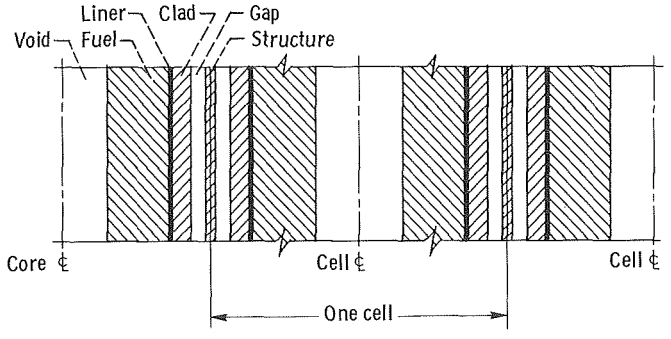

(a) Cut through core at structure contact points.

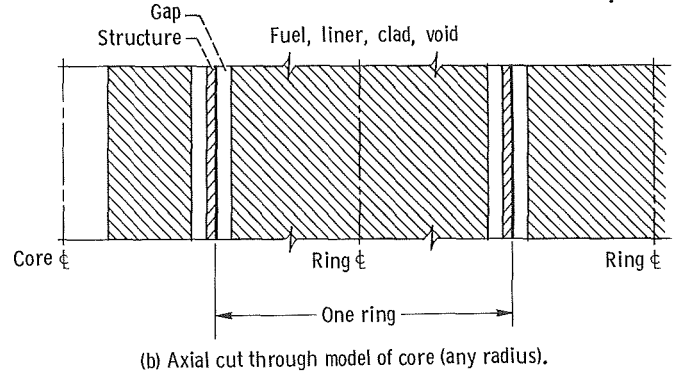

(b) Axial cut through model of core (any radius).

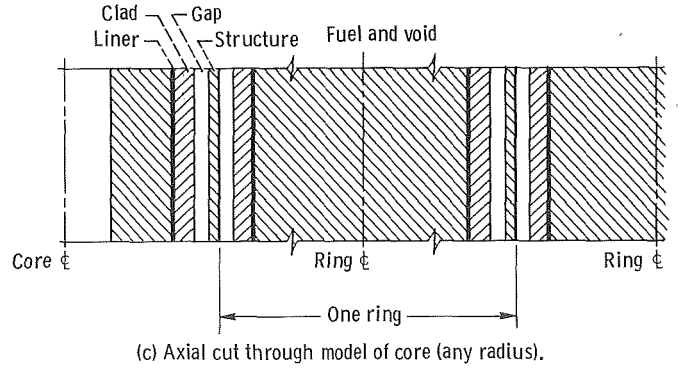

(c) Axial cut through model of core (any radius).

Figure 21. - Ring model of radial cut through core.

heat conductive and heat radiative regions. Since modeling radiative heat transfer in such a complicated geometry is a difficult task to perform accurately, three models were chosen for these studies:

(1) Steady-state core model (fig. 21(b)) - a one-dimensional model through the core for steady-state temperature distribution calculations; fuel, liner, clad, and void treated together in one region.

(2) Kinetic core model (fig. 21(c)) - a one-dimensional model through the core for the kinetics studies of power and temperature transients; fuel, liner, and clad treated in separate regions in order to properly represent the reactivity effect of each region.

(3) Adiabatic cell model (fig. 3 without coolant) - a one-dimensional model through an average cell for kinetics studies of the core, which neglects heat-transfer effects between cells and out of core; fuel, liner, and clad in separate regions for good heat transfer and reactivity feedback modeling.

The cores of the two core models are modeled by a succession of rings of cells. Each ring (fig. 15(b)) is approximately one cell diameter in width. Each ring is subdivided specifically to represent the radiation gap between the fuel and structure. In figure 21 the axial cut along a radius through the structure contact points of the cells is shown in part (a). Part (b) shows the model for the steady-state calculations. Because of the small temperature difference across the fuel and clad compared with that across the adjacent gaps and the absence of reactivity effects in a steady-state calculation, the individual effects of fuel, liner clad, and central void are unimportant. Hence these materials are treated together in one region. The center of each ring is the average radius to the centers of all cells included in the ring. Within each ring the real gap (0.102 cm or 0.040 in.) across the void and the real thickness (0.051 cm or 0.020 in.) of the structure at contact points were maintained, and the fuel region thickness is adjusted accordingly. Thermoconductivities are governed according to the masses and volumes involved. Figure 21(c) is the model for calculation of transients. It is the same as (b) except that the liner and clad regions are separated from the fuel region for more realistic reactivity feedback simulation. Another model for the kinetics analysis uses a single adiabatic cell to represent the core; this model is the same cell shown in figure 3, but with the coolant removed. In the kinetics analysis the model shown in figure 3 provides an accurate description of the thermodynamics of the cell, but the model shown in figure 21(c) compromises on in tracellular heat transfer to give information about heat flow across and out of the core.

Equations

The nodal network set up in AIROS for model (3) is shown in figure 22. The feedback equations for this model are (subscripts refer to nodes marked in fig. 22)

$$\frac{dT_1}{dt} = \frac{H_1}{(\rho C_p V)_1} N(t) - \frac{(UA)_{12}}{(\rho C_p V)_1} (T_1 - T_2) \tag{11}$$

$$\frac{dT_2}{dt} = \frac{(UA)_{12}}{(\rho C_p V)_2} (T_1 - T_2) - \frac{(UA)_{23}}{(\rho C_p V)_3} (T_2 - T_3) \tag{12}$$

$$\frac{dT_3}{dt} = \frac{(UA)_{23}}{(\rho C_p V)_3} (T_2 - T_3) - \frac{\sigma \epsilon A_3}{(\rho C_p V)_3} \left(T_3^4 - T_4^4\right) \tag{13}$$

$$\frac{dT_4}{dt} = \frac{\sigma \epsilon A_3}{(\rho C_p V)_4} \left(T_3^4 - T_4^4\right) \tag{14}$$

The nonlinear radiative heat-transfer terms could not be programmed in the original version of AIROS, so it was modified to handle T^p terms in general. The kinetics and reactivity equations (5) to (8) apply here also.

The nodal model in figure 22 and the feedback equations (13) to (15) are easily extended to describe the more complicated models (a) and (b) of figure 21.

Cell

Fuel	Liner	Clad	Structure
U^{235}	W	T-111	T-111
U^{235} Dop	W Dop	W, Ta } Dop	W, Ta } Dop
		Fuel, Core } Axial Exp	(Core radial Exp)
		(Core radial Exp)	
1	2	3	4

Figure 22. - Nodal model for adiabatic cell without coolant. Doppler (Dop) and thermal expansion (Exp) reactivity effects are placed in the node whose temperature controls the effect. Those in parentheses are used only in special cases as explained in the section Results. Numbers at bottom are node numbers used as subscripts in feedback equations (11) to (14).

Results

Steady-State. - Four cases are considered

(1) T_{sink} = 294 K (530° R); flat power distribution

(2) T_{sink} = 294 K (530° R); realistic power distribution

(3) T_{sink} = 294 K (530° R); realistic power distribution; all materials in outer ring treated together in one region, thus removing radiative heat transfer from center core ring

(4) T_{sink} = 461 K (830° R); flat power distribution

All four cases are represented together in figure 23 for steady-state operation at 200 watts.

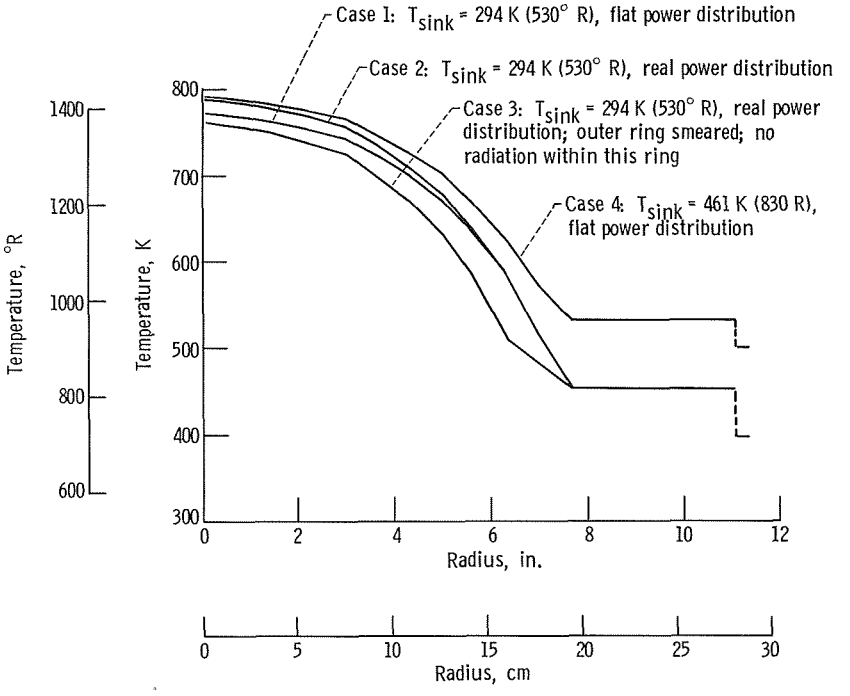

Figure 23. - Temperature distributions in different cases of 200-watt steady-state operation.

At this level the difference between the maximum core temperatures in the 294 and 461 K sink-temperature cases 1 and 4 is 20 K (36° R). As shown in figure 24, at low power levels (≥0.02 W) the difference between the maximum core temperatures approaches the difference between the sink temperatures; at high power levels (≥20 kW) the

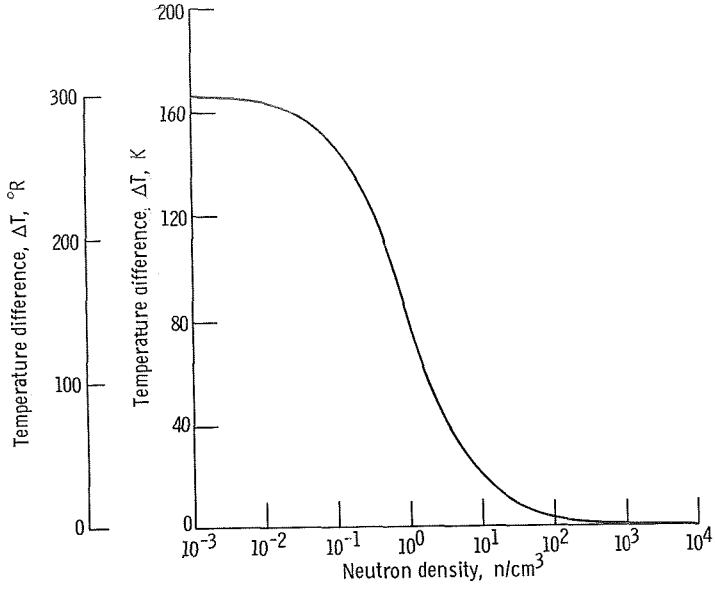

Figure 24. - Difference between maximum core temperatures for 294 and 461 K (530° and 830° R) sink temperature cases.

difference in maximum core temperatures approaches zero, even though the sink temperatures are different.

As shown in figure 23, the temperature distribution is affected more by the modeling than by the power distribution. Since the fuel elements occupy only about half the volume of the outer ring, heat transfer is divided between conduction and radiation. Thus cases 2 and 3 should provide bounding curves for the real temperature distribution. In the core itself, heat conduction through the honeycomb structure will represent only a small part of heat transfer because of the small cross section for heat conduction. This effect is entirely neglected in these problems, which tends to make the results slightly conservative.

The normalized real power distribution (as determined from the two-dimensional transport program (TDSN; ref. 8) calculations of neutron density distribution) and the temperature distributions for various power levels are plotted in figure 25. Because of the vacant coolant channels and reduced heat flow, the temperature gradients in the core are much steeper than in the reactor containing coolant. In the normal reactor with coolant flow at full power, the temperature difference radially across the core is about 67 K (120° R). It is not much different when the coolant is not flowing, and the same average temperature is maintained because of the high thermal conductivity of the liquid metal. However, with the coolant absent the temperature difference across the core is about 500 K (900° R) at 2000 W and 280 K (500° R) at 200 W.

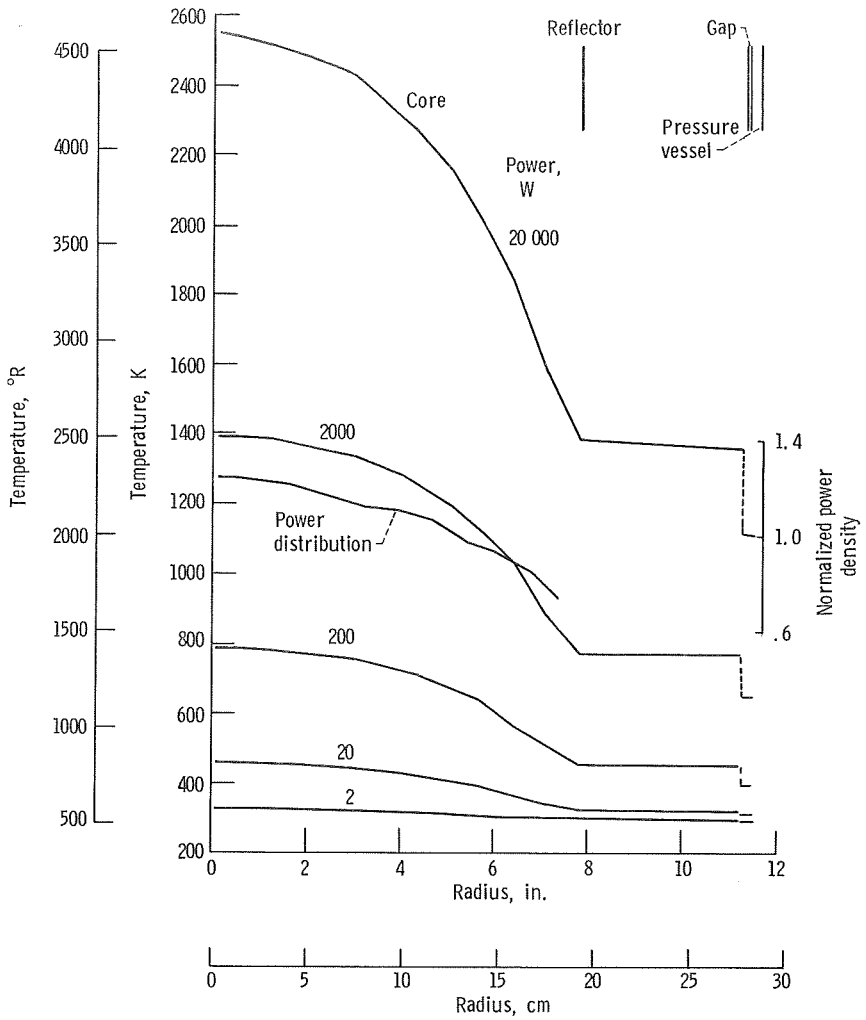

Figure 25. - Temperature distribution in HCA at steady state with no coolant present. Case 2 (T_{sink} = 294 K).

The most conservative case for a given sink temperature has the power distributed realistically, and it is used to determine the upper limit of operation at steady-state, which is controlled by the melting point of UN (2910 K or 5260° R). Extrapolating the maximum temperatures (see fig. 25) to 2910 K yields a 30-kW limit, which is well above normal operating levels in critical experiments.

Transients. - Using the adiabatic cell rather than the whole HCA (models (b) and (c)) was necessary and sufficient for this investigation. The adiabatic cell accurately pro-

vided the correct thermodynamic model for intracellular heat transfer although it assumed that no heat was lost from the cell. Model (b) verified that the cells are antonomous thermodynamically for the range of transients studied here. Hence the results presented here were gained entirely from the adiabatic cell model.

An extreme set of results for the study of the effects of ramp rate and ramp level on fuel temperature are shown in figure 26 for the adiabatic cell with axial fuel and core expansion effects of table II, but with no radial core expansion. In comparing this with figure 11 (which has radial core and coolant expansion effects present) we find that in both cases the critical ramp rate is 9 ¢/sec, and both have the same four types of regions;

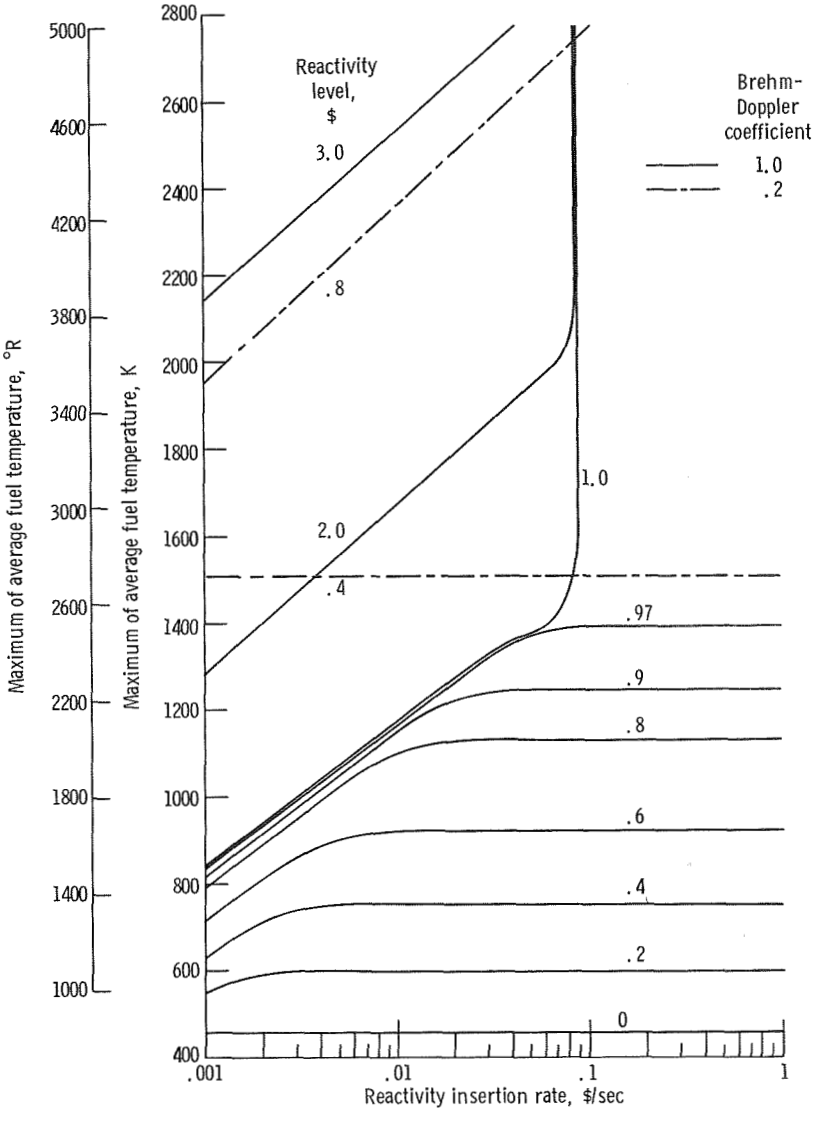

Figure 26. - Sensitivity of fuel temperature transients to ramp reactivity inputs. HCA without coolant. Startup from delayed critical with all temperatures at 461 K (830° R). Initial power, 20 watts. Clad expansion coefficients, -4×10^{-4} \$/K (-2×10^{-4} \$/°R). See table III for Doppler coefficients.

however, the step input region begins at lower ramp rates when the coolant is absent. Most striking in figure 26 are the higher temperatures reached by lower reactivity input levels. Lacking the reactivity effect of the coolant and deprived of a faster response from the structure temperature (and hence the Doppler feedback) due to the decreased ability of the cell to transfer heat from the clad to the honeycomb structure, the HCA suffers higher temperatures for the same reactivity input when the coolant is taken out.

Some typical transients for the adiabatic cell without coolant are shown in figure 27.

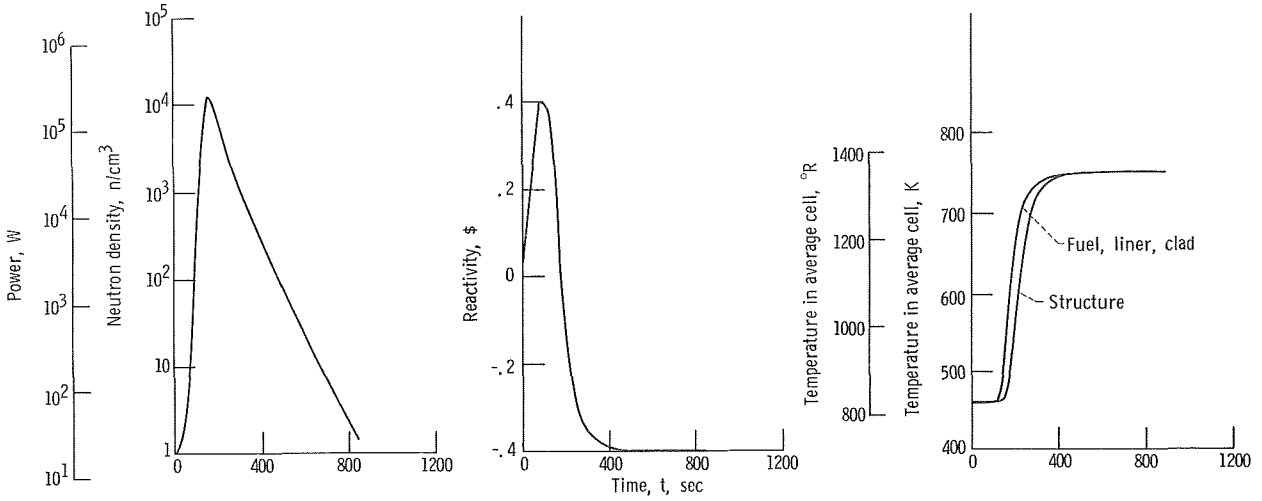

(a) Power transients. (b) Reactivity transient. (c) Temperature transients.

Figure 27. - Typical transient for HCA without coolant. Reactivity input rate, 0.5 ¢/sec to 40 ¢. Clad expansion coefficient, -4×10^{-4} \$/K (-2×10^{-4} \$/°R). See table III for Doppler coefficients.

Since the cell is adiabatic, the maximum temperature reached is of course the final, steady-state temperature, reached as the HCA is shutdown by the feedback effects. Absent from the transients are the initial peaks which signaled an approach to the critical ramp rate in the HCA with coolant.

The situation shown in figure 26 is a pessimistic view of the HCA since no radial core expansion was accounted for. A more realistic model associates the core expansion coefficient with the structure or clad temperature. This will lead to a higher maximum safe reactivity input level than is shown in figure 26. These effects are examined in the following paragraphs.

Core expansion may take place in two ways. It is normally associated with the structure, but, if there is clearance between the honeycomb structure and the fuel, some fuel and clad expansion can take place as the clad temperature increases. If the fuel elements are assumed to be lying towards the center of the core, the fuel expansion within the clearance between it and the honeycomb structure results in a net core expansion equal to the expansion of the diameter of the fuel elements in the outer perimeter of the

core. Since the fuel element diameter is about one-tenth of the core radius, the core expansion coefficient associated with the clad temperature is only one-tenth as great as the core expansion coefficient associated with the structure temperature.

The effects of the core expansion coefficient in raising the maximum safe reactivity input level are shown in figure 28. Whether all the core expansion effect is associated

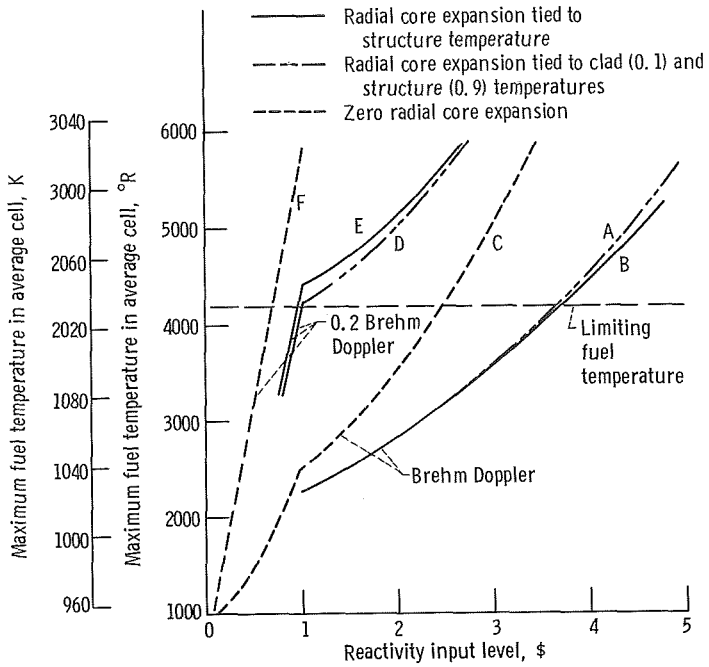

Figure 28. - Maximum safe reactivity input levels for HCA without coolant.

with the structure temperature or one-tenth of it is associated with the clad temperature has little effect on the maximum safe reactivity input, as the differences between curves A and B or D and E attests. The two pairs differ by the amount of Doppler assumed: curves A and B are for the Brehm computed coefficients and curves D and E and for 0.2 of those values. Curves C and F provide reference points for the hypothetical cases of zero Doppler effect. Being conservative about it, one would pick curve E as the limiting case, with the maximum safe reactivity input set at 97 ¢.

The ability of the HCA to shut itself down by inherent feedback mechanisms is shown in the behavior of transients in figure 27. Shutdown margins for the situations plotted in figure 28 vary between 80 ¢ and 1.7 $.

CONCLUSIONS

The safety aspects of the kinetics of a hot critical assembly (HCA) have been investigated for startup conditions, presumed to be the least safe of all operating conditions. It is concluded that an HCA can be operated safely with only a minimum of restrictions on its operating capabilities. The most conservative, yet realistic, limitations on reactivity inputs, which will prevent possible fuel melting, are given in the following table:

For a drum-controlled HCA with a single drum worth about 2.5 $, operation is inherently safe if all the following conditions are met:

1. HCA is full of coolant.
2. Only one drum is moved at a time.
3. The Drum rate is restricted to less than 9 ¢/sec.

Operation of an HCA without coolant requires either a positive interlock which prevents any drum from inserting 0.95 $ or a redesign in which each drum is worth less than 0.95 $.

Wide variations in the reactivity coefficients will affect neither the critical ramp rate (9 ¢/sec) nor the maximum safe reactivity insertion at rates above the critical rate, because of the time delays of the feedback mechanisms. At rates below the critical rate, the limits of the maximum safe reactivity input will be modified when more exact values of the Doppler and expansion coefficients become available.

Lewis Research Center,
National Aeronautics and Space Administration,
Cleveland, Ohio, May 27, 1970,
120-27.

APPENDIX A

SYMBOLS

A_i	area of right cylindrical surface with radius r_i and length equal to that of fuel element, m^2; ft^2
B_i	reactivity coefficient for feedback temperature T_i in region i
C_i	neutron precursor population, nuclei/m^3
C_p	heat capacity, J/(kg)(K); Btu/(lb)(^oR)
f_i	fraction of delayed neutrons attributable to precursor group i
H_i	thermal power production coefficient for region i, (J)(m^3)/(n)(sec); (Btu)(ft^3)/(n)(sec)
k	neutron multiplication factor
ℓ	prompt neutron lifetime, sec
$\text{Min}(\gamma_1 t, \gamma_2)$	ramp function with slope γ_1 and level γ_2, \$
N	neutron density, n/m^3; n/ft^3
r	reactivity = $(\delta k/k)/\beta$, \$
T_i	temperature in region i, K; ^oR
t	time, sec
U	overall coefficient of heat transfer, J/(sec)(m^2)(K); Btu/(sec)(ft^2)(^oR)
V	volume, m^3; ft^3
β	fraction of delayed neutrons
γ_1	slope of reactivity input ramp, \$/sec
γ_2	input reactivity ramp level, \$
δT_i	shape function of temperature reactivity feedback in region i
ϵ	emissivity for radiative heat transfer
λ_i	decay constant for precursor group i, sec^{-1}
ρ	density, kg/m^3; lb/ft^3
σ	Stefan-Boltzmann constant for radiative heat transfer, J/(sec)(m^2)(K^4); Btu/(sec)(ft^2)($^oR^4$)
τ	thermodynamic time constant, sec

APPENDIX B

DOPPLER COEFFICIENTS

Brehm (ref. 4) studied the Doppler coefficients for several materials used in fast reactors and determined the following formulas emprically (for $\beta = 0.0068$):

For T in K and $\partial r/\partial T$ in \$/K

$$\left.\frac{\partial r}{\partial T}\right|_{235} = 0.147\, I^2\, T^{-1}$$

$$\left.\frac{\partial r}{\partial T}\right|_{238} = -0.131(1 - I)^2\, T^{-0.8}$$

$$\left.\frac{\partial r}{\partial T}\right|_{W} = -0.0902\, \frac{M^W}{M^{235}}\, T^{-0.8}$$

$$\left.\frac{\partial r}{\partial T}\right|_{Ta} = -0.484\, \frac{M^{Ta}}{M^{235}}\, T^{-0.8}$$

For T in ^{o}R and $\partial r/\partial T$ in \$/^{o}R

$$\left.\frac{\partial r}{\partial T}\right|_{235} = 0.147\, I^2\, T^{-1}$$

$$\left.\frac{\partial r}{\partial T}\right|_{238} = -0.116(1 - I)^2\, T^{-0.8}$$

$$\left.\frac{\partial r}{\partial T}\right|_{W} = -0.0802\, \frac{M^W}{M^{235}}$$

$$\left.\frac{\partial r}{\partial T}\right|_{Ta} = -0.430\, \frac{M^{Ta}}{M^{235}}$$

where

$\left.\frac{\partial r}{\partial T}\right|_m$ Doppler effect due to material m

T absolute temperature

I enrichment of fuel (atomic fraction of U^{235} to total uranium)

M^m mass of material m

These formulas are based on infinite dilution ratios of activities of a given material to that of U^{235} and a rule of thumb for U^{235} worths which is 0.5 percent $\delta M/M$ where M is the critical mass of U^{235} in a fast reactor. If significant self-shielding is involved, the Doppler effect will be estimated too high.

REFERENCES

1. Blaine, R. A.; and Berland, R. F.: AIROS: A Digital Simulator for Power Reactor Dynamics. Rep. NAA-SR-9943, Atomics International, Aug. 1, 1964.

2. Kreith, Frank: Principles of Heat Transfer. Second ed., International Textbook Co., 1965, p. 129.

3. Nakache, F. R.: Review and Evaluation of Temperature-Induced Feedback Mechanisms in Fast Power Reactors. Rep. UNC-5054, United Nuclear Corp., Apr. 1, 1963.

4. Brehm, Richard L.: Estimates of Doppler Coefficients for In-pile Thermionic Reactor Materials. Tech. Rep. 32-1077, Jet Propulsion Lab., California Inst. Tech. (NASA CR-85358), Oct. 1, 1967.

5. Burdi, G. F.: SNAP Technology Handbook. Rep. NAA-SR-8617, Atomics International, 1965.

6. Davison, Harry W.: Preliminary Analysis of Accidents in a Lithium-Cooled Space Nuclear Powerplant. NASA TM X-1937, 1970.

7. Shaver, R. E.; and Wittenbrock, N. G.: Review of Reactor Safety Analyses of Fast and Liquid Metal Cooled Reactors. Rep. BNWL - 477, Battelle-Northwest, Nov. 1967.

8. Barber, Clayton E.: A Fortran IV Two-Dimensional Discrete Angular Segmentation Transport Program. NASA TN D-3573, 1966.

NASA-Langley, 1970 — 22 E-5289

NATIONAL AERONAUTICS AND SPACE ADMINISTRATION
WASHINGTON, D.C. 20546

OFFICIAL BUSINESS

FIRST CLASS MAIL

POSTAGE AND FEES PAID
NATIONAL AERONAUTICS AND
SPACE ADMINISTRATION

POSTMASTER: If Undeliverable (Section 158 Postal Manual) Do Not Return

"The aeronautical and space activities of the United States shall be conducted so as to contribute . . . to the expansion of human knowledge of phenomena in the atmosphere and space. The Administration shall provide for the widest practicable and appropriate dissemination of information concerning its activities and the results thereof."

—NATIONAL AERONAUTICS AND SPACE ACT OF 1958

NASA SCIENTIFIC AND TECHNICAL PUBLICATIONS

TECHNICAL REPORTS: Scientific and technical information considered important, complete, and a lasting contribution to existing knowledge.

TECHNICAL NOTES: Information less broad in scope but nevertheless of importance as a contribution to existing knowledge.

TECHNICAL MEMORANDUMS: Information receiving limited distribution because of preliminary data, security classification, or other reasons.

CONTRACTOR REPORTS: Scientific and technical information generated under a NASA contract or grant and considered an important contribution to existing knowledge.

TECHNICAL TRANSLATIONS: Information published in a foreign language considered to merit NASA distribution in English.

SPECIAL PUBLICATIONS: Information derived from or of value to NASA activities. Publications include conference proceedings, monographs, data compilations, handbooks, sourcebooks, and special bibliographies.

TECHNOLOGY UTILIZATION PUBLICATIONS: Information on technology used by NASA that may be of particular interest in commercial and other non-aerospace applications. Publications include Tech Briefs, Technology Utilization Reports and Notes, and Technology Surveys.

Details on the availability of these publications may be obtained from:

SCIENTIFIC AND TECHNICAL INFORMATION DIVISION

NATIONAL AERONAUTICS AND SPACE ADMINISTRATION

Washington, D.C. 20546